

REPORT DOCUMENTATION PAGE			Form Approved OMB No. 0704-0188	
<small>Public reporting burden for this collection of information is estimated to average 1 hour per response, including the time for reviewing instructions, searching existing data sources, gathering and maintaining the data needed, and completing and reviewing the collection of information. Send comments regarding this burden estimate or any other aspect of this collection of information, including suggestions for reducing this burden, to Washington Headquarters Services, Directorate for Information Operations and Reports, 1215 Jefferson Davis Highway, Suite 1204, Arlington, VA 22202-4302, and to the Office of Management and Budget, Paperwork Reduction Project (0704-0188), Washington, DC 20503.</small>				
1. AGENCY USE ONLY (Leave Blank)		2. REPORT DATE 5/16/96		3. REPORT TYPE AND DATES COVERED Final Report
4. TITLE AND SUBTITLE Measurement of Strain at Interior Points Using Synchrotron Radiation			5. FUNDING NUMBERS G#F49620-92-J-0204	
6. AUTHOR(S) Eric H. Jordan and Douglas M. Pease			AFOSR-TR-96 0281	
7. PERFORMING ORGANIZATION NAME(S) AND ADDRESS(ES) University of Connecticut Dept. of Mechanical Engineering Storrs, CT 06269				
9. SPONSORING/MONITORING AGENCY NAME(S) AND ADDRESS(ES) AFOSR/NA 110 Duncan Ave. Suite B115 Bolling AFB, DC 30332-0001 NA			10. SPONSORING/MONITORING AGENCY REPORT NUMBER 92-J-0204	
11. SUPPLEMENTARY NOTES				
12a. DISTRIBUTION/AVAILABILITY STATEMENT Unlimited 19960617 124				
13. ABSTRACT (Maximum 200 words)  A method was developed for measuring strain on interior surfaces of optically opaque objects using synchrotron X-ray radiation. Images of small markers (20 micron) were recorded before and after straining using the special properties of synchrotron radiation. Strain is determined by measurement of the change in markers spacing using a special electro-optical method. Gage lengths of 100 microns are currently used and the strain resolution is on the order of 100 micro strain. The first generation version of the technique was used to study composite material behavior and some interesting results were obtained. Finite element studies were conducted to show that markers should be at least 5 diameters apart to avoid marker induced stiffening effects. A greatly improved second generation technique was largely developed. Improvements resulted in order of magnitude increase in the area recorded per radiograph and in the speed of processing the results. These improvements were based on the development of a new marker fabrication technology and a redesigned automated marker positioning measurement system. Measurement error and reliability was also improved. The method can be used for samples up to the atomic number of titanium. One additional minor improvement is needed to begin full utilization of the method.				
14. SUBJECT TERMS Internal, Strain Measurement, Composites, X-Ray, Synchrotron Micromechanics			15. NUMBER OF PAGES 165	
			16. PRICE CODE	
17. SECURITY CLASSIFICATION OF REPORT U	18. SECURITY CLASSIFICATION OF THIS PAGE U	19. SECURITY CLASSIFICATION OF ABSTRACT U	20. LIMITATION OF ABSTRACT U	

# DISCLAIMER NOTICE



**THIS DOCUMENT IS BEST QUALITY AVAILABLE. THE COPY FURNISHED TO DTIC CONTAINED A SIGNIFICANT NUMBER OF PAGES WHICH DO NOT REPRODUCE LEGIBLY.**

## **MEASUREMENT OF STRAIN AT INTERIOR POINTS USING SYNCHROTRON RADIATION**

### **ABSTRACT**

A method was developed for measuring strain on interior surfaces of optically opaque objects using synchrotron X-ray radiation. Images of small markers (20 micron) were recorded before and after straining using the special properties of synchrotron radiation. Strain is determined by measurement of the change in markers spacing using a special electro-optical method. Gage lengths of 100 microns are currently used and the strain resolution is on the order of 100 micro strain. The first generation version of the technique was used to study composite material behavior and some interesting results were obtained. Analytical and finite element studies were conducted to show that markers should be at least 5 diameters apart to avoid marker induced stiffening effects on the measured strain. A greatly improved second generation technique was largely developed. In the first generation technique x-ray pictures were taken as a non uniformly exposed mosaic picture by using a standard monochromatized synchrotron beam (0.6 mm X 50 mm). In the second generation technique a greatly enlarged more uniform beam (10 mm X 33 mm) has been produced by using a channel cut asymmetric crystal monochromator. With the improved radiographic technique it is possible to record more than 30,000 markers in a single radiograph. To take advantage of the increased area an affordable method of producing large arrays of uniformly spaced nickel markers was developed. The uniform location of the new markers provided an opportunity to automatically map the position of 100's of markers on enlarged images of the radiographs. To achieve this automation, a dramatic improvement in the electro-optical position measuring systems was necessary and was achieved by the use of fiber optics and by a total system redesign. This system has demonstrated a reduced noise strain of 50 micro strain. The one remaining technical problem to be solved is the development of a method for removing the thin metal film from between the markers. This film because of its high modulus will unduly reinforce the plane bearing the markers compared to the polymer material in which they are embedded. Further work is planned to solve this remaining problem to bring the improved method into full operation.

### **Introduction**

The measurement of strain is a highly developed technology. For surface locations, existing methods range from point measurements via strain gages to highly automated full field method such as phase shifted Moire' (1). Measurement of strain at interior locations of optically transparent materials is possible by both frozen photo elasticity (2) and by white light speckle holography (3). None of these method however allows for measurement of strain at interior locations in optically opaque materials. The goal of the current program Air Force Grant # F49620-92-0204 "Measurement of Strains at Interior Points Using

Synchrotron Radiation" was to develop a new technique to accomplish this task. The feasibility of the new method was demonstrated under this program and the first generation experimental technique was used to study composite materials. . A second generation method was also nearly completed that will increase by more than an order of magnitude the amount of data collected with a single radiograph and also will also increase the rate of data reduction by at least an order of magnitude.

The steps in the method are illustrated in Figure 1. Small (20 micron) metal markers are embedded on a plane of interest inside of the object. The special properties of synchrotron X-ray radiation are used to form images of these markers before and after mechanical loading. The radiographs are optically enlarged and then very carefully measured to determine the change in marker spacing. Strain is then computed by differentiation of the measured marker coordinates.

An important consideration in such measurements is the potential disturbance of the strain field being measured by the high modulus markers. Calculations show ( Appendix I) that if the markers are 5 diameters apart the strain errors are less than 1%. Consequently, minimization of gage lengths requires minimizing the size of the markers used.

The properties of synchrotron radiation are critical for forming x-ray images of minimum sized markers. These x-ray images are shadow pictures in which objects are made visible by the difference in absorption properties compared to the surroundings. Three properties of synchrotron radiation are important to imaging small markers. First, synchrotron radiation is well collimated which allows small x-ray shadow features to be observed without stray x-rays from other angles weakening or exposing the shadow (figure 2). Second, synchrotron radiation can be selected at the wave length for which the marker material has maximum absorption. The optimum wave length typically results in an absorption coefficient that is 10 time as large as non optimum wave lengths. Markers must be thick enough to block a large enough fraction of x-rays to form an image of adequate contrast. Selection of optimum wavelength allows significantly thinner markers to be used. Because marker fabrication is limited in aspect ratio, thinner markers can be smaller markers and hence shorter gage lengths may be used. Third, synchrotron beams are nearly parallel resulting in very uniform , one-to-one imaging. This is important because variations in magnification would appear as false strains.

### **Demonstration of Feasibility Using 1 st Generation Technique**

During this program the new method was subject to extensive verification testing and then it was applied to problems in graphite epoxy laminated composites. A complete description of this work is given in Appendix II. This testing showed that the typical noise strain is somewhat less than 100 micro strain on a gage length of about 200 microns. In the original version of the method, markers were created by painting a slurry of small gold particles on the desired surface. All measurement of marker positions before and after straining were made one marker coordinate at a time using an electro-optical set-up. This set-

up used an X-Z stage, a laser, and a biaxial position sensing diode (see fig. 3). A interesting result achieved with this version of the technique is shown in Figure 4. In this experiment an 8 layer [+45/-45/-45/+45]s graphite epoxy plate with a hole was tested. Markers were placed on its mid plane. On the left in fig. 4, the normalized strain distribution near the hole is shown for a moderate load. The measured strain distribution is close to several theoretical strain distribution in the plate at a higher load is shown on the right in figure 4. The scale for both the ordinate and abscissa are different on the right half of figure 4 compared to the left half. The higher load for the case shown on the right in this figure was sufficient to produce local delamination. The extreme disruption of the strain distribution is clearly shown even through no damage was obvious on visual inspection. The strain distribution in the damaged panel is nearly impossible to compute because of the complex geometry of delamination and due to the fact that the delamination geometry details are not known. This work established that strains could be measured by the technique and that useful, unique results could be obtained. Finally the technique was shown to be capable of imaging markers in boron aluminum composites. Unfortunately the boron fibers were grown on tungsten cores that obscured all but a few markers.

Experience with the technique was encouraging, however it became apparent that an improved method of creating the markers was needed. Specifically, it was found that mixing gold particles with a liquid and painting process to get a marker density where the markers were about 5 diameters apart. If the marker density was higher than the ideal, the high modulus (gold) markers would disrupt the strain field being measured ( Appendix I), while too low a density resulted in sparse data and long gage lengths. Even careful weighing of materials when mixing particles for painting does not guarantee ideal results because the gold settles out of solution during painting. The markers were various shapes and sizes and an unknown fraction of them would not show up on the radiographs. In addition, the random placement of markers sometimes resulted in a lack of usable markers in the key area of interest. Manual measurement of the marker coordinates was tedious and time consuming. As a result, the data in fig. 4 involves only about 10 measured strains. It was decided that two improvements would be of great value. First, a method to make uniform sized, uniformly spaced markers was needed. Second, an automated method of measuring the marker positions was needed. A major effort was directed toward this surprisingly difficult task.

## **Development of 2nd generation technique**

### **Improved X-ray image recording**

The synchrotron x-ray beam used to make radiographs was that from a double bounce monochromator and was about 0.6 mm X 50 mm . Reasonable area radiographs were made as mosaics that had very non uniform exposure Fig. 5. It was highly desirable to obtain radiographs with more uniform exposure. X-ray beams can be enlarged by using a single crystal where the free surface and the Bragg planes are not parallel. In such monochromators the angle monochromator incidence measured from the free surface and angle of reflection are not equal. With proper design such asymmetric reflecting monochromators give enlarged beams and improved intensity uniformity. Such a monochromator was designed and fabricated under the current program. A proposal for using an existing beam line which already had

such a monochromator was also successful. Dramatic improvement in exposure uniformity and area covered in the radiograph was achieved as shown in Figure 6. Figure 6 shows a fraction of a radiograph made with an asymmetric monochromator. The markers appear as transparent areas on a dark opaque background on both the original radiograph negatives and on slides of the negatives used in measuring strain. The markers shown in fig. 6 appear black on a white background because of the photo process used to make this print. The dramatic improvement in exposure uniformity and area coverage is apparent in the comparison of fig. 5 and fig. 6. It is worth noting that for the process shown in fig. 5 only 6 columns of markers could be recorded in one radiograph.

#### Improved electro-optical setup.

The current system for measuring marker spacing suffered from air current effects on the optical path and pointing instability of the laser. Coupling the laser to an optical fiber removed the effects of pointing drift and also allowed the measurement system to sit vertically reducing air current effects. When the fiber optic source was used in the existing set up, small temperature changes combined with optical leverage effects produced serious beam positional instability. The set up in fig. 3 is especially susceptible as nonuniform growth in the height of the component holders which produces a loss of alignment of the whole system. It was further observed that air currents deflected the beam producing further positional noise. In manual mode one could wait for quite moments to make measurements however automation was infeasible in the presence of these instabilities. The set up was redesigned to have a vertical beam path with an axisymmetric configuration and minimal air gaps, these changes nearly eliminated the thermal misalignment effects and dramatically reduced air current effects. A schematic of the new electro-optical setup is shown in figure 7. To test the system, a sample dot pattern was repeatedly measured and the strain which was actually zero was computed. The noise strain had a maximum value of 50 micro strain. The improved system allowed automatic strain mapping with good accuracy.

A computer program was written to compute the strain from the measured marker positions. This software was developed by a high school summer student visiting the university as part of an enrichment program. The computer program had to deal with missing markers that occasionally occur and with imperfect alignment of the marker pattern primary axis of the positioning stage.

#### Improved Marker Fabrication

The metal markers required for making high contrast radiographs must be about 20 micron thick for gold and 30 microns thick for nickel. This thickness was calculated and experimentally verified. Careful analytical studies and finite element analysis showed that markers must be 5 diameters apart in order to get undisturbed strain readings (appendix 2). We choose as an ambitious but achievable goal the fabrication of a rectangular array of 20 micron diameter markers 100 microns apart. Small diameter markers with the same thickness would lead to better spatial resolution in strain measurement but would be much more difficult and expensive to fabricate. It is worth noting that circuit board conductors a typical maximum thickness of 2 microns. The technology for the fabrication of small metal features

20+ microns thick is not particularly well developed. We will briefly describe some unsuccessful fabrication methods considered. This information will be useful to others attempting to advance the technique. The successful methods will then be presented.

Initial attempts were made using photo resist masking and the thermal evaporation of gold. It was possible to create a pattern of holes in a thick photo resist and by running the evaporator for days at a time it was possible to deposit thick gold into the pattern. Unfortunately in all but a few cases the gold came off when the photo resist was lifted off. One good specimen was made which had 14 micron thick gold markers however it was found that this sample yielded x-ray images too low in contrast for the measurement of strain. Attempts were made to put down patterns using gold infiltrated paste applied using a screen mask. Marker patterns were made but the gold flakes in the paste did not pack densely enough and thickly enough to yield usable patterns. Attempts at selective etching of nickel were made however the markers detached from the substrate.

Two successful marker fabrication methods were developed. First 25 micron deep hole patterns were laser drilled commercially. These holes cost about \$0.05/ea. Drilling a full square inch of 64,000 holes would cost about \$3200 however a smaller array of holes was drilled. Thermal evaporation of gold into the holes for 3 days produced marker thicknesses of roughly 20 microns and good contrast x-ray images were produced. Second, plastic samples were covered with 1500 angstroms of nickel by evaporation. The evaporation coating was quite inexpensive. Following this, a pattern of nickel markers was fabricated by a commercial electroforming company. The process involves producing a photo resist mask and then electroforming on to the nickel layer with an electrochemical process. Excellent full coverage samples were formed at a cost of about \$100/each. The resulting marker pattern sits on top of the 1500 angstrom nickel layer. The nickel layer because of its high stiffness will effect strain measurement if not removed. All attempts to date to remove this layer by etching failed due to passivation of the nickel. Successful etch removal of the thin nickel layer is the focus of our current unfunded efforts.

#### Status of the second Generation Experimental Technique

Samples with electroformed nickel markers were tested on a visit to the synchrotron. The 1500 nickel layer was present on these samples and the markers were on the free surface. Excellent high contrast images were obtained as shown in fig. 6. It was observed optically that under straining the markers were detaching at random locations in the pattern but remained attached to the thin nickel sublayer at other locations. The resulting strain maps showed large variations in computed strain as would be expected for a mixture of attached and detached markers. The marker detachment problem would be eliminated for embedded markers however because the nickel has a modulus that is on the order of 100 times that of the plastics used, the thin layer would have a significant reinforcing effect. Accordingly current efforts are directed at removing the thin nickel layer between the markers.

#### Educational Effects

This program supported in substantial part the education of two graduate students who both happened to be from under represented minorities. Simian Ochi received his Ph.D in 1991 based on a thesis on the development of this new technique. Dr. Ochi now is employed at

Cooper Tire company. Angel Rivera received an MS degree working on this program. Mr Rivera is now employed by the General Electric company. One high school student spent a summer on this project as part of an enrichment program. And undergraduate Christopher Perry made a significant portion of the money needed to self finance his B.S. degree in Mechanical Engineering. The educational impact of the project was significant and relevant as indicated by the perfect placement record for students involved in the project.

## Summary

An entirely new strain measurement technique useful for measuring strains inside of optically opaque objects was developed under the current program. The first generation technique achieved:

1. 100 micro strain resolution on a 100 micron gage length for the measurement of strain at interior locations in optically opaque objects.
2. Analytical and finite element results were obtained showing that markers should be 5 diameters apart in order that the stiff markers do not unduly disturb the strains being measured.
3. The technique provided some interesting results for composite materials. Strain measurements were in good agreement with two out of three analytical solutions for strain near a hole. Strains near a hole following local delamination were measured and found to be dramatically disturbed. The strain disturbance revealed damage not otherwise apparent.
4. The feasibility of strain measurement in aluminum boron composites was demonstrated. Strain measurement for higher atomic number metals than titanium is not likely to be successful.

A second generation technique was developed. This technique will be further developed beyond the current program. The new technique has improved on the first generation technique as follows

1. An order of magnitude increase in the area covered by a single radiograph with dramatically more uniform exposure was achieved through the use of asymmetric channel cut single crystal monochromator.
2. Dramatic improvement in the stability of the system used to measure marker position was achieved. This in turn enabled full automation of strain mapping from marker images. The new system also reduced strain noise levels from about 100 micro strain to 50 micro strain.
3. A practical affordable marker fabrication technique was developed where a square inch pattern with 64,000 markers can be made for approximately \$100. Current work is on finding

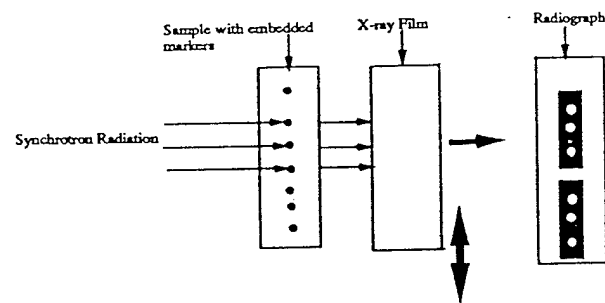
a method to remove the thin metal layer from between markers is ongoing. The removal of this layer is desirable due to the effect of that layer has on strain in the much lower modulus plastics being studied.

Two under represented minority graduate students were educated and both have excellent jobs. It is the expectation of these investigators that the second generation technique will be fully successful and unfunded work is continuing along with efforts to obtain further funding to complete its development.

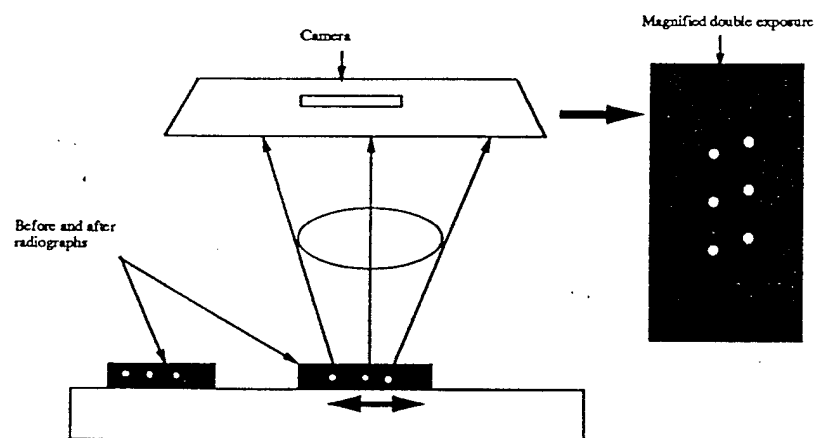
#### References

1. Perry, K. E. and McKelvie, "Measurement of Energy Release Rates for Delaminations in Composite Materials, Experimental Mechanics V. 36, No. 1, pp 55-63.
2. Dally, J. W. and Riley, W. F. , Experimental Stress Analysis, 3rd ed. New York : McGraw-Hill, inc. 1991.
3. Chiang, F. P. and Asundi, A. , "White Light Speckle Method of Experimental Strain Analysis, Applied Optics", Vol 18, PP 409-411.

## Step 1



## Step 2



## Step 3

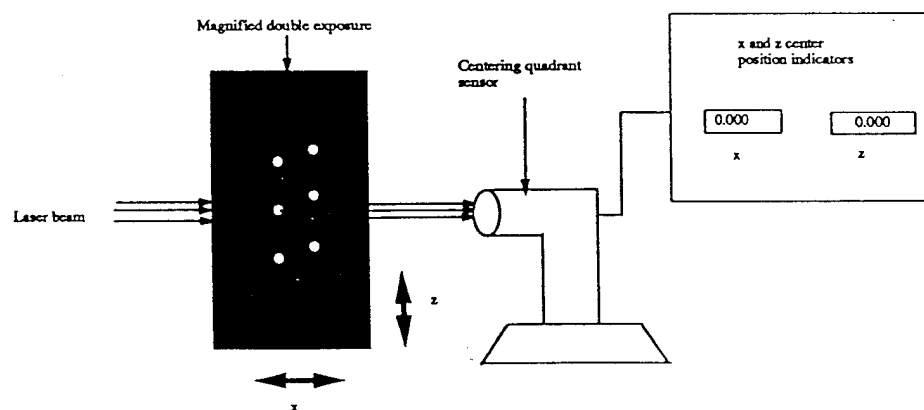
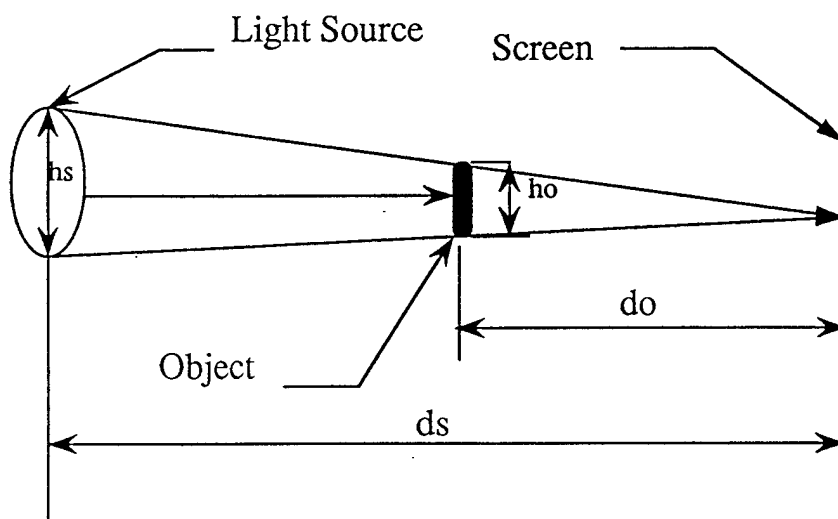
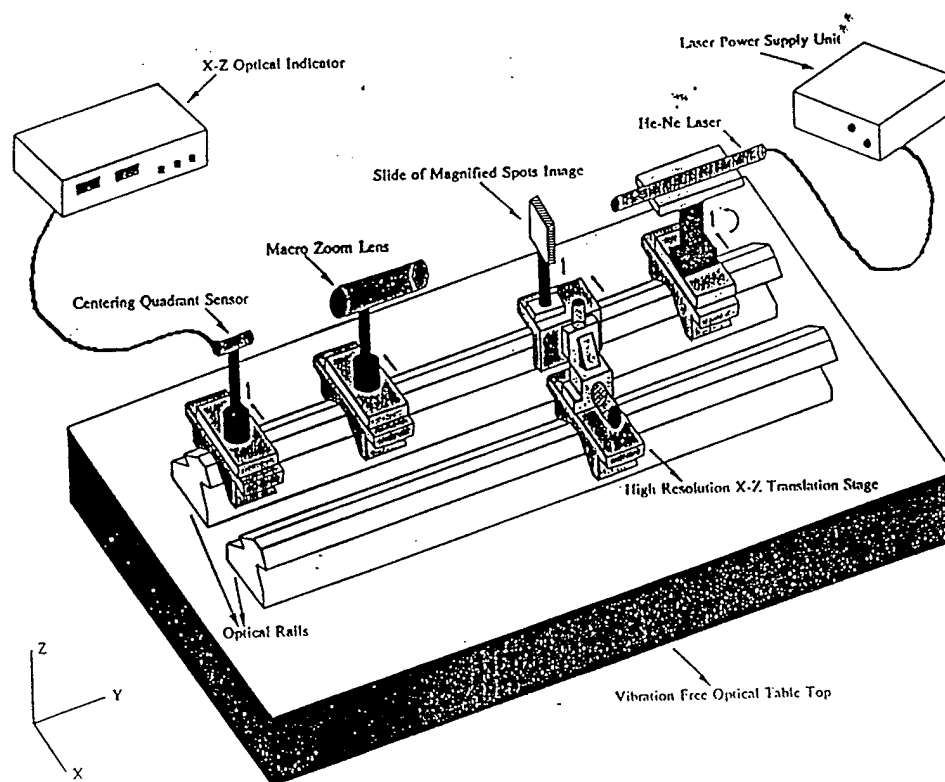


Figure 1. Block diagram of how the new experimental technique works.



From Similar triangles  $ho = h_s \times (do/ds) = \text{minimum object size}$

**Fig. 2 Shadow Fill in With Uncollimated Source.**



**Fig. 3 First Generation Electro-optical System for Measuring Inter-marker Spacing**

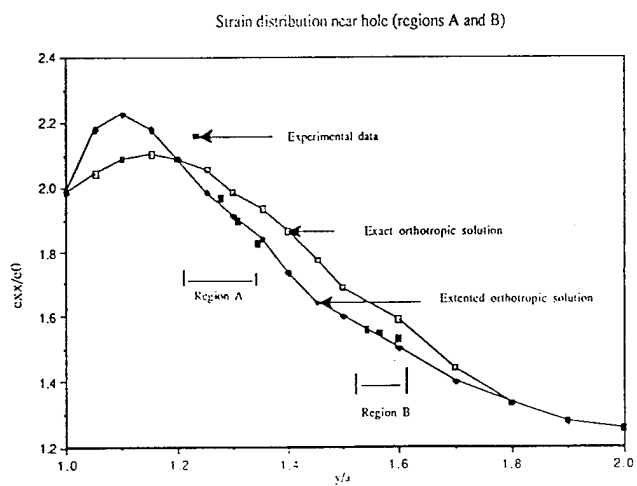
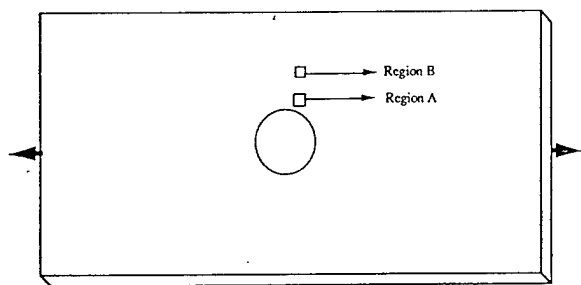


Fig. 4a Elastic Load.

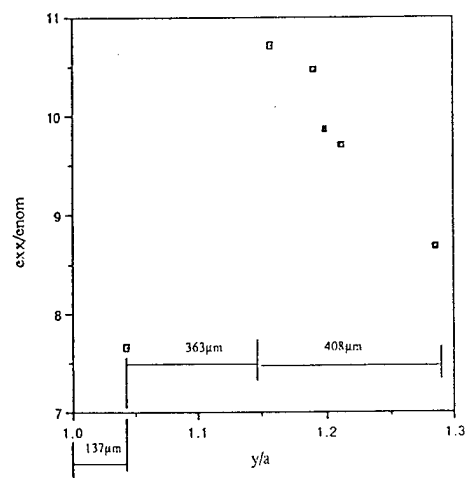
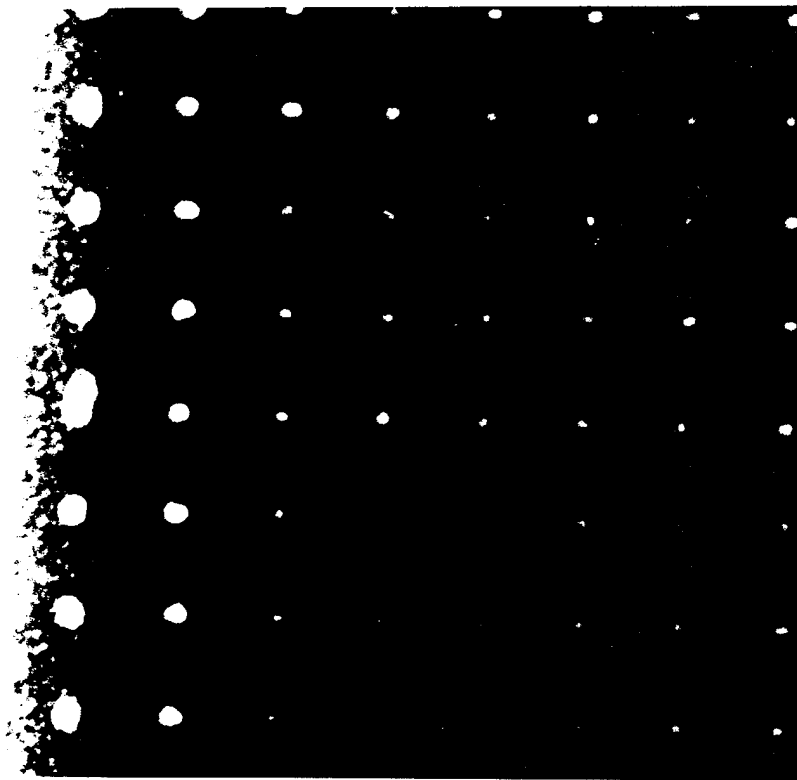
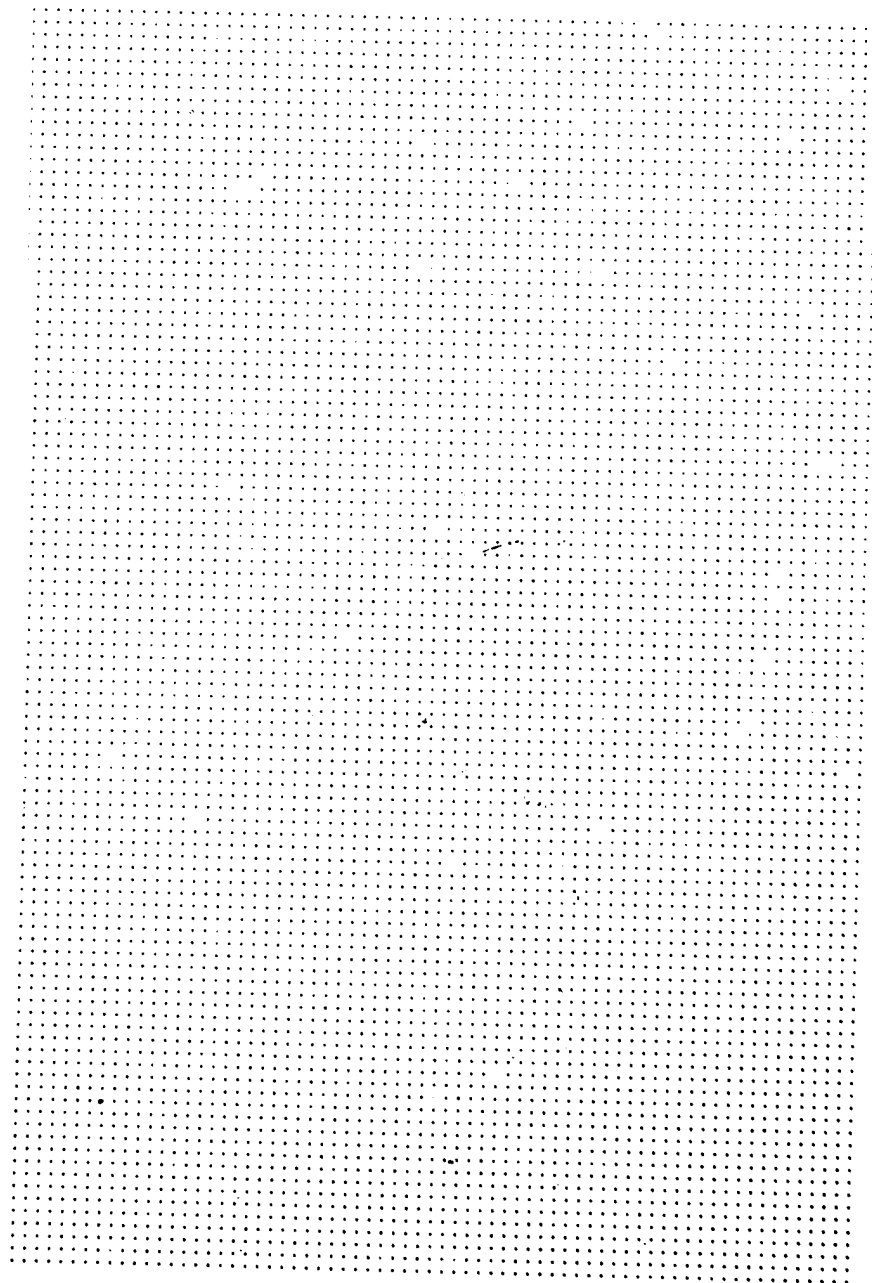


Fig. 4b Near Delamination Load.



**Fig. 5 Mosaic Radiograph of Gold Markers in a Lap Joint.**



**Figure 6. Enlarged radiograph of markers using the improved asymmetric monochromator.**

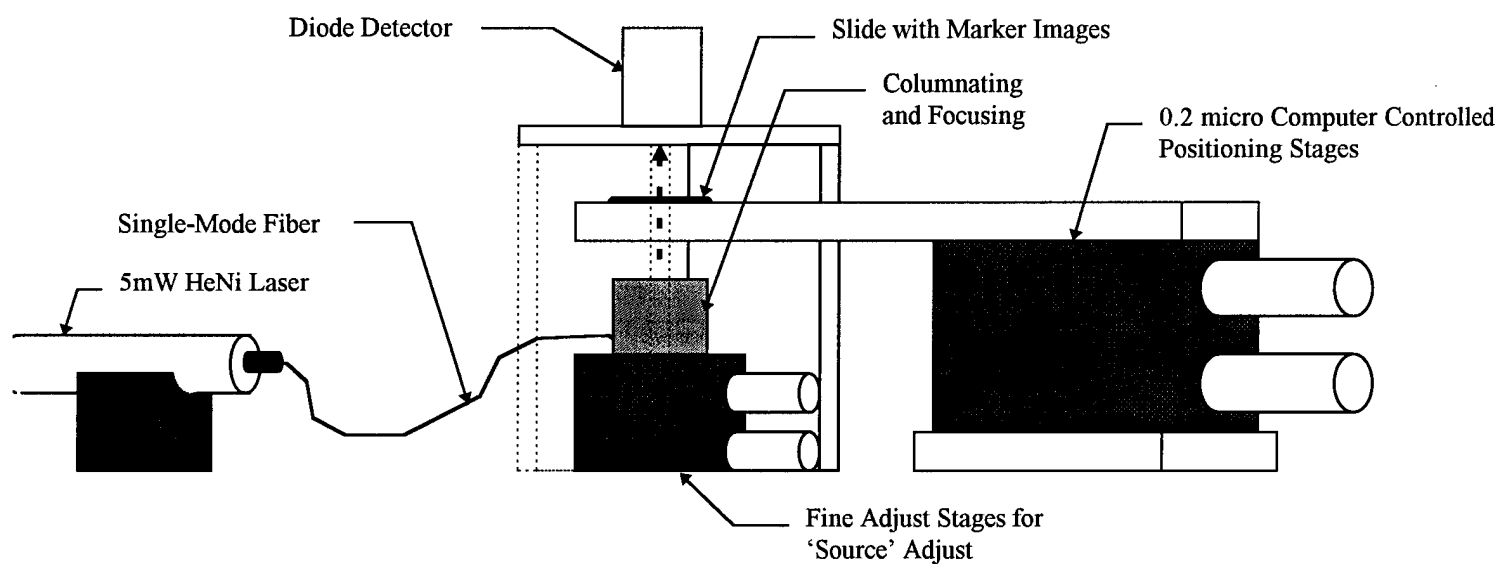


Fig. 7 - 2nd Generation Electro-Optical Marker Spacing Measurement System.

## **Appendix I-Influence of Embedded Markers on the Response of the Host Material**

## Influence of Embedded Markers on the Response of the Host Material

Authorized Reprint from Journal of Testing and Evaluation May, 1995

Copyright 1995 American Society for Testing and Materials, 1916 Race Street, Philadelphia, PA 19103

**REFERENCE:** Ochi, S. C. U., Accorsi, M. L., and Jordan, E. H., "Influence of Embedded Markers on the Response of the Host Material," *Journal of Testing and Evaluation*, JTEVA, Vol. 23, No. 3, May 1995, pp. 196–202.

**ABSTRACT:** The effect of embedded marker particles on global stiffness and strains determined when using these markers as fiducial marks is studied analytically. These effects are important to a recently developed strain measurement method that uses before and after X-ray pictures of the embedded marker particles. Global effect of the markers on the stiffness is studied using micromechanical models available from the literature. The error in the measured strain due to the influence of the markers is assessed by both the finite element method and elasticity theory. It is shown that the global influence is small for marker-volume fractions less than 3%. The induced strain measurement error is small for particles that are five or more marker-diameters apart. A simple formula for the strain measurement error in the case of particles that are five or more marker-diameters apart is derived from elasticity theory.

**KEYWORDS:** embedded markers, host material, smart materials

Techniques for the measurement of internal material response as well as for monitoring and controlling their behavior using embedded distributed sensors are actively being developed. Passive materials such as fiber optic fibers embedded in the structure are used to monitor internal material response. In these applications, the fibers are interrogated using a laser and the phase changes of the beam as it passes through the fibers during deformation of the host medium are used for calculating internal material response. Example fiber-sensor systems developed for determining distributed strain as well as structural vibration mode-shape amplitudes are given in Refs 1 to 3.

Recently, Jordan et al. [4] developed a new experimental technique for measuring internal strains in structural materials using well-collimated X-ray source (synchrotron radiation) and spherical marker particles. In this method, the passive marker particles which are highly absorbing of X-rays are embedded on one plane of the sample and the X-ray images of the positions of the marker particles before and after deformation are used to determine the strain fields in the medium. This technique has a strain resolution of 100  $\mu$ strain on a 300- $\mu$ m gage length and it has been used, for example, to

measure interlaminar strain distributions in the interior of graphite-epoxy composites.

This new technique shares with the other embedded sensor techniques a common concern of how to account for the disturbance introduced by the presence of the sensors or the markers when measuring the structural response of the host material. A complete understanding of how the markers influence the response of the host media is crucial to the validity of the method. The motivation for this paper is, therefore, to develop a relevant analytical technique to examine both global and local influences of the markers on the structural response of the host media. Analytical and numerical solutions for determining both global and local influence of the presence of marker particles as they relate to the new method will be presented.

The influence of the presence of the sensors on the response of the host material as it pertains to other techniques has been treated in varying aspects by others. Measures et al. [5] noted that the presence of embedded optical fibers did not compromise the tensile and ultimate strengths of crossply composites and also did not have a detrimental influence on the materials' resistance to delamination. However, Czarnek et al. [6] demonstrated in experimental interferometric Moire measurements of the displacement fields surrounding an optical fiber that strain concentrations higher than 10-to-1 occur within the optical fiber-matrix interface region for specimens that are loaded to approximately half their failure loads. It is further observed that although such concentrations may be relatively unimportant in large composite structures, the interface site may be a logical initiation site for internal cracks and thus of potential concern for the long-term integrity of the host structural component. Haslach and Whipple [7] analytically studied designs of embedded fibers and concluded that for tensile loads less than 100 MPa, the separation distance between two adjacent fibers must be at least four coating diameters in order that they will sense the strain as though the other fibers were not there.

The works of the researchers in Refs 5 to 7 on the influence of the sensors on the structural response of the host material are different from that of Jordan et al. [4] not only with respect to the geometry of the markers but also with respect to gage lengths. With the exception of the errors introduced by the mechanical interaction of the markers and the host material, all other sources of strain error measurements in the method were treated by Jordan et al. [4]. In this paper, calculations are carried out to assess the significance of two types of undesirable effects of the markers used in strain measurement. First, the influence of markers on the effective stiffness of the layer in which the markers are placed is

Manuscript received 9/6/94; accepted for publication 11/14/94.

<sup>1</sup>Vehicle analysis specialist, Cooper Tire and Rubber Company, Auburn, IN 46706.

<sup>2</sup>Associate professor of civil engineering and professor of mechanical engineering, respectively, University of Connecticut, Storrs, CT 06269.

considered. This may be important, for example, in a symmetric laminate where a change in layer stiffness can produce unwanted extensional-flexural coupling. Second, the question of strain measurement error that occurs by virtue of the marker particles changing the strain field that is being measured is considered.

In the case of calculating the change in average effective properties, effective properties expressions derived from volume averaging elastic solutions of idealized geometries are used. Calculations are conducted for specific composites of interest to the authors and the method of calculation could be used by others for other cases. The results show that while the global strain error is only moderately sensitive to the volume fraction of the markers, it is very sensitive to the ratio of the marker modulus to the host material modulus being studied. However, regardless of moduli ratio, if the volume fraction of markers is less than 1%, the global stiffness change is less than 1%.

The local error introduced in the strain measured due to the presence of the markers is first studied for the dilute case by solving the elasticity problem of a single marker embedded in an isotropic matrix. Subsequent finite element analysis (FEA) shows that the simple formula for the dilute case is sufficiently accurate for cases in which the particles are five marker-diameters apart. The error as a function of particle spacing is such that those desiring high accuracy measurements will only be concerned with the relatively dilute case for which the simple formula is adequate. The FEA is also used for studying local strain error when the host material is being plastically strained.

### Global Influence of Markers on the Response of the Host Materials

In this section, the influence of the presence of the spherical markers on the global structural response of the host composite or homogeneous media will be examined. The approach is simply to compare the effective material properties of the host material containing a prescribed percentage of the markers to its original properties. We analyzed the influence of spherical markers on the effective properties of aluminum-boron and graphite-epoxy composites with low volume fraction (20%) of fibers. These composites are also candidate materials for the experiment and the markers are embedded on a plane of interest of the composites prior to heat consolidation. In the analysis, we used the composite cylinders model [8] to calculate the effective elastic properties of each composite. To account for the spherical markers in the fiber-reinforced medium, a three-phase model [9] was used, where a spherical marker is surrounded by a layer of matrix that is embedded in an infinite medium with the effective properties of the composite. The effect of adding 1% to 10% volume fraction of nickel or gold spherical markers to the original material was then evaluated. Schematics of these models are shown in Fig. 1.

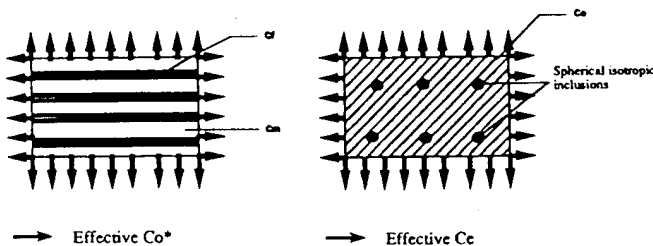


FIG. 1—(a) Fiber-reinforced composite, (b) homogenized media containing spherical inclusions.

Percentage change of the global response of the host medium due to the markers was found using the following expression:

$$\Delta\epsilon_{ij}(\%) = \frac{100(C'_{ij} - C^o_{ij})}{C^o_{ij}} \quad (1)$$

where  $C^o_{ij}$  and  $C'_{ij}$  are material properties with and without the markers, respectively.

The results for the error introduced in values of the uniaxial stiffness components of graphite-epoxy and aluminum-boron composites after adding 1% to 10% volume fraction of the markers are shown in Figs. 2 and 3, respectively. These results show that while the global strain error is only moderately sensitive to the volume fraction of the markers, it is very sensitive to the ratio of the modulus of the host material  $E_h$  to the modulus of the marker  $E_m$ . The strain error sensitivity to the moduli ratio is further illustrated by Fig. 4 showing variation of strain error at 1% and 3% volume fraction.

In the experimental technique as currently implemented, the volume fraction is approximately 0.11%. At this volume fraction, it is reasonable to conclude that the global influence of the markers on the structural response of the host medium is insignificant.

### Local Influence of Markers on the Response of the Host Materials

The presence of one or more inclusions or voids in an elastic medium introduces a disturbance of the structural response of the

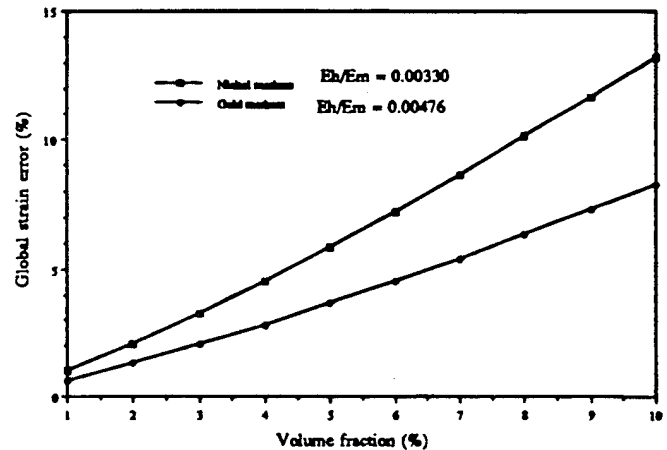


FIG. 2—Global strain error for graphite-epoxy composite.

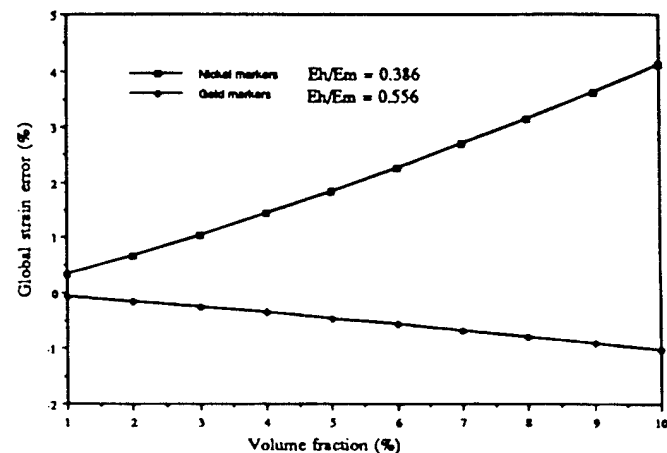


FIG. 3—Global strain error for aluminum-boron composite.

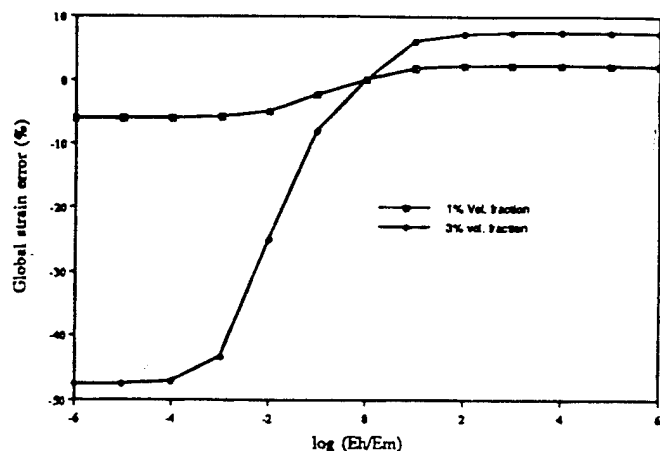


FIG. 4—Global strain error for 1% and 3% marker volume fractions.

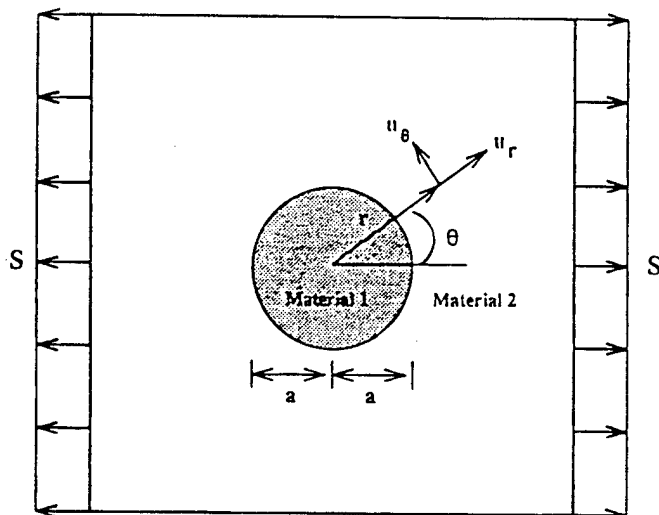
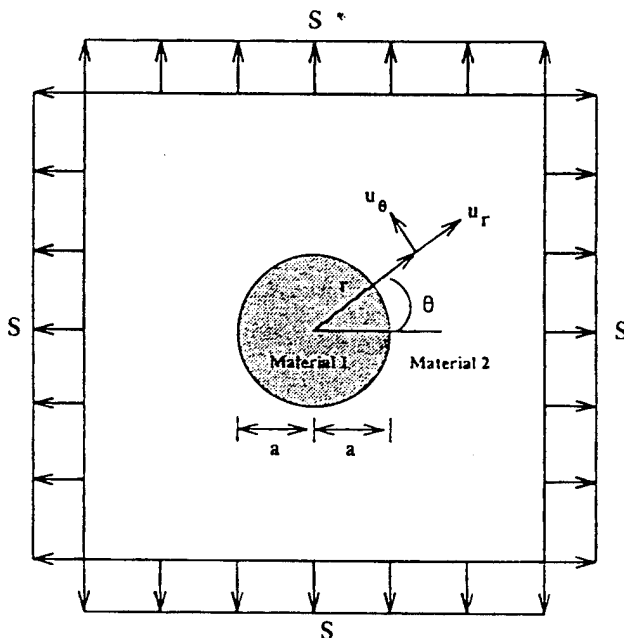
host medium. The disturbance is local as shown in Refs 10 and 11. Literature review of elasticity solutions of an infinite linear elastic medium containing two rigid inclusions or voids reveals that the optimum separation distance between the inclusions is reached when the principal stress/strain concentration at each inclusion-medium interface is approximately equal to that prevailing when there is only one inclusion or void present in the medium. For an infinite linear elastic medium containing two spherical rigid inclusions or cavities treated in Refs 12 to 14, the optimum distance is between 2.5 and 3 inclusion-diameters, while it is 2 inclusion-diameters for a plate under tension containing two circular holes treated in Ref 15.

The problems presented in Refs 12 to 14 were concerned with examining stress concentration as a function of the spacing between two rigid inclusions contained in an infinite medium. In the present problem, however, we are using the elastic inclusions as fiducial markers and we are interested in how their presence influences strain values calculated from the markers relative displacements. In our approach we shall first determine the closed-form solution of the disturbance introduced by one marker in the host medium and use this solution to estimate the disturbance introduced by two or more noninteracting markers. Second, we shall use the finite element method to calculate the disturbance introduced in the strain field when there are two or more interacting markers in the medium.

#### Closed-Form Solution

In this section, the local influence of one marker on the response of its medium will be estimated using the average strain calculated at a field point located far away from the marker. To estimate the local influence of two or more noninteracting markers on the field point, we simply superimpose the local fields. It will turn out that the analysis of the average strain error derived from the solution for a medium containing one marker will be sufficient for estimating the influence of markers located relatively far from one another.

An infinite elastic medium containing one circular marker is selected for analysis. The medium is treated for both uniform uniaxial and biaxial tension applied at infinity as shown in Figs. 5 and 6. Uniaxial loading has many obvious applications but biaxial loading is also relevant because the experimental technique can be used for measuring strain relaxation in residual stress fields. Because of the circular geometry of the marker, we adopt from Refs 10 and 11 the stress and other functions in polar coordinates.

FIG. 5—Infinite elastic medium containing one marker subjected to uniform uniaxial tension  $S$ .FIG. 6—Infinite elastic medium containing one marker subjected to uniform biaxial tension  $S$ .

Plane stress conditions are assumed in each case because a typical sample is 2 mm thick containing spherical markers of 20 to 40  $\mu\text{m}$  in size. The stress problem at hand will be solved using the Airy stress function approach. Here we will present a summary of the solution for the case shown in Fig. 5. Details of this solution can be found in Ref 16. The stress functions are

$$\phi_1(r, \theta) = \frac{S}{4} \left( A_1 r^2 + B_1 r^2 \cos 2\theta + \frac{C_1 r^4 + \cos 2\theta}{a^2} \right) \quad (2)$$

$$\phi_2(r, \theta) = \frac{S}{4} \left( r^2 - r^2 \cos 2\theta + A_2 a^2 \log r + \frac{B_2 a^4 \cos 2\theta}{r^2} + C_2 a^2 \cos 2\theta \right) \quad (3)$$

where the subscripts 1 and 2 refer to the marker and the medium, respectively.

Upon applying the boundary conditions and solving, the radial displacement in the host medium  $u_{r2}$  has the following form:

$$u_{r2} = \frac{S}{2\mu_2} \left[ (K_2 - 1)r + 2r \cos 2\theta - A_2 \frac{a^2}{r} + 2B_2 \frac{a^4}{r^3} \cos 2\theta + (K_2 + 1) C_2 \frac{a^2}{r} \cos 2\theta \right] \quad (4)$$

where

$$A_2 = \frac{-2[r(K_1 - 1) - K_2 + 1]}{r(K_1 - 1) + 2} \quad (5)$$

and

$$B_2 = \frac{-(5rK_1 + 6)(r - 1)}{3(3r + 2K_2)(rK_1 + 1)} \quad (6)$$

$$C_2 = \frac{4(r - 1)}{3r + 2K_2} \quad (6a)$$

where

$$r = \frac{\mu_2}{\mu_1} \quad K_1 = \frac{3 - \nu_1}{1 + \nu_1} \quad (6b)$$

are the constants of integration,  $K$  is the plane stress parameter, and  $\mu$  is the shear modulus, respectively.

Using the center of the marker as a reference point, and noting that its displacement is zero, the average strain at any arbitrary field point  $p$  located a distance  $r$  away from the marker can be defined as

$$\epsilon_p^r = \frac{u_{r2} - 0}{r} \quad (7)$$

which on substitution for  $u_{r2}$  becomes

$$\epsilon_p^r = \frac{S}{2\mu_2} \left[ (K_2 - 1 + 2 \cos 2\theta) - A_2 \frac{a^2}{r^2} + 2B_2 \frac{a^4}{r^4} \cos 2\theta + (K_2 + 1) C_2 \frac{a^2}{r^2} \cos 2\theta \right] \quad (8)$$

for one marker.

The strain error can be found by subtracting the undisturbed far-field strain to yield the following expression for the strain disturbance of the marker

$$\Delta\epsilon(\%) = -100 \left[ A_2 \frac{a^2}{r^2} - 2B_2 \frac{a^4}{r^4} \cos 2\theta + (K_2 + 1) C_2 \frac{a^2}{r^2} \cos 2\theta \right] \quad (9)$$

Equation 9 represents the change due to the marker in the average strain measured from the marker's center to a point at location  $r$ . If a second marker is placed at  $r$  then, by superposition the change in the average strain will be twice that of Eq 9 if interaction is ignored. This estimate is valid for a medium containing sparsely dispersed markers. Thus, the error in determining the strain as a function of the length change between the two markers divided by their separation when  $p$  is located on the line of centers is approximated as follows:

$$\Delta\epsilon(\%) = -2 \times 100 \left[ A_2 \frac{a^2}{r^2} - 2B_2 \frac{a^4}{r^4} \cos 2\theta + (K_2 + 1) C_2 \frac{a^2}{r^2} \cos 2\theta \right] \quad (10)$$

When  $r = 10a$ ,  $\theta = 0$ ,  $A_2 = 1.0$ , and  $B_2 = 0.5$ , and  $C_2 = -1.00$  (corresponding to a nickel marker in an epoxy host material), the error is approximately 2%.

In the experiment, we use a multitude of markers to capture the strain field. We can extend this estimate of strain error to an actual sample by considering a geometric pattern of ten markers located around two markers A and B as shown in Fig. 7. When the markers are not interacting with one another, the strain error imposed on the A-B pair is

$$\Delta\epsilon(\%) = -100 \times \left[ 4A_2 \left( 1 - \frac{1}{\sqrt{2}} \right) \frac{a^2}{r^2} + \frac{3}{5} B_2 \left( \frac{1}{\sqrt{2}} + \frac{1}{\sqrt{5}} \right) \frac{a^4}{r^4} \right] \quad (11)$$

Using identical parameters applied to Eq 10, the error is approximately 1.2%. This estimated error is lower than in the previous case because the angular arrangement of the markers around the fiducial pair is such that some terms cancel out.

We shall postpone further discussion of Eqs 10 and 11 until we have the results of the finite element model, which include marker interactions.

#### Finite Element Solution of Local Influence of Two or More Interacting Markers

The finite element model of the material containing two markers used in this study is shown in Fig. 8. The analysis was performed using the MARC finite element code together with MENTAT pre- and post-processor. To simulate constant uniaxial strain throughout the medium, the model was subject to a uniform displacement applied to the top edge of FE model as shown in the figure. Symmetry boundary conditions are applied on the remaining boundaries. Four-noded and eight-noded isoparametric quadrilateral elements were used in the marker and host material regions, respectively. Aluminum-boron (Al-B) and graphite-epoxy (Gr-Epxy) host materials containing nickel and gold markers were analyzed.

The error in the calculated strain using the differential displacements is defined, in percentage terms, as

$$\Delta\epsilon(\%) = 100 \left( \frac{\epsilon_m - \epsilon_u}{\epsilon_u} \right) \quad (12)$$

where  $\epsilon_u$  is the uniform strain in the medium in the absence of

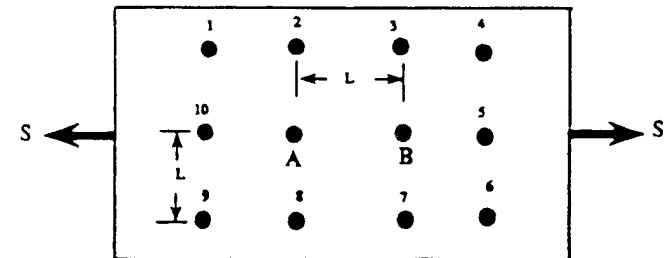


FIG. 7—Markers A and B surrounded by ten neighboring markers representative of typical marker pattern in an actual sample.

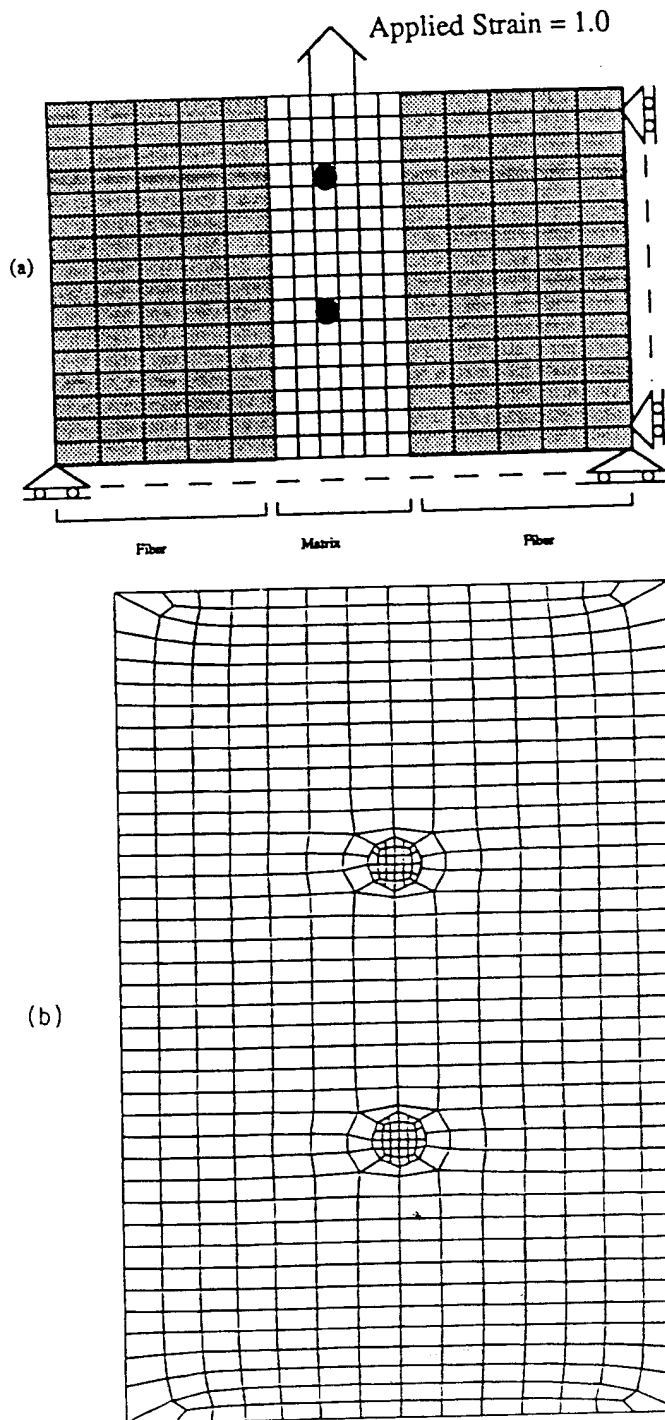


FIG. 8—(a) Composite material containing two markers, (b) corresponding finite element model.

the markers and  $\epsilon_m$  is the strain calculated using the relative displacements of the two markers defined as

$$\epsilon_m = \frac{u_{m2} - u_{m1}}{g_1} \quad (13)$$

where the quantity  $g_1$  is the separation distance along the line of centers between the markers or the local gage length, and  $u_{m1}$  and  $u_{m2}$  are the displacements of markers 1 and 2, respectively.

## Discussion of Results

We start the discussion by comparing the elasticity and finite element solutions of a uniform medium containing one marker. The strain field results are plotted in Fig. 9, and as expected, the two solutions agree very well. The error from the introduction of the two markers into the medium are shown in Figs. 10a and 10b for nickel-epoxy and gold-aluminum material systems, respectively. The finite element result represents the case when the two

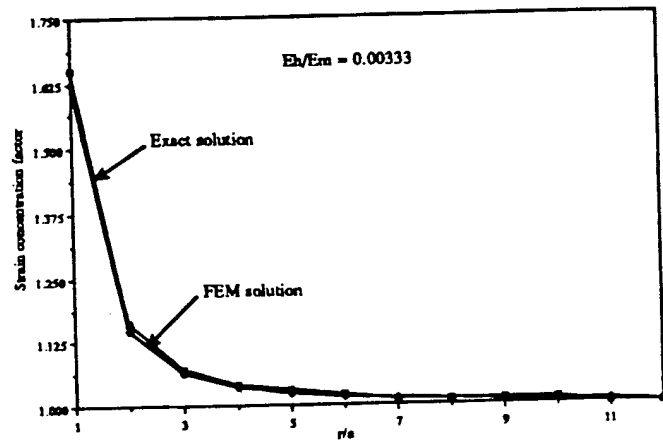


FIG. 9—Strain concentration factor for host epoxy material containing one nickel marker.

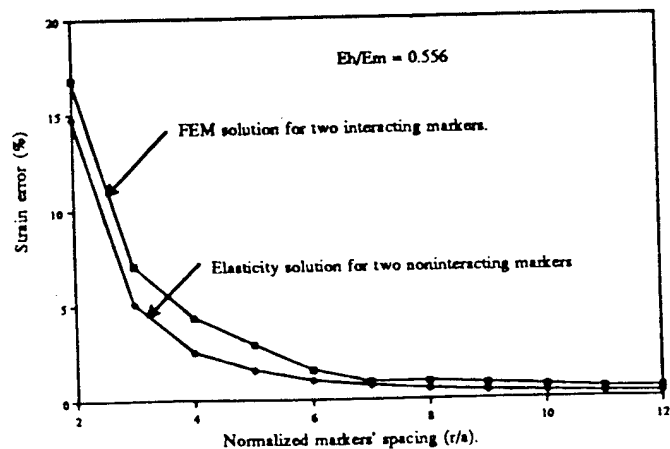
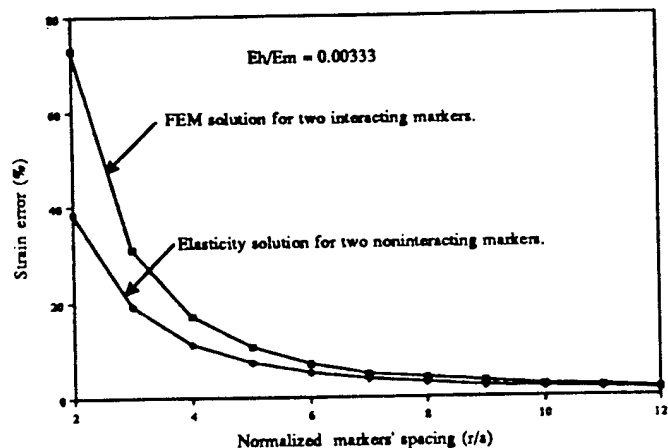


FIG. 10—Local strain error (a) two nickel markers in epoxy host material, (b) two gold markers in aluminum host material.

markers are interacting as given by Eq 12, and the elasticity result represents the case of noninteracting markers as given in Eq 10. From the figures, it can be observed that the two local disturbance fields progressively decrease with an increase in  $r$ ; at  $r/a \approx 10$ , the error is about 2.5% in Fig. 10a, and 0.65% in Fig. 10b. Also, notice that the local disturbance dominates the response of the host material, when  $r/a = 2$ , that is, when the two markers are touching. For this particular case in the FE model, the two markers act as one element and there is very little relative displacement between them. It is also noted in Refs 12 to 14 that the mathematical solution of the local stress field used does not converge when the two inclusions are touching.

Some important findings in this study are: (1) for a marker-material system with extreme values of the moduli ratio (for example in nickel-epoxy system  $E_f/E_m \approx 10^{-3}$ ), the error introduced by the local disturbance is approximately 2.5%, when  $r/a = 10$ ; (2) for a marker-material system with moderate moduli ratio (example, gold-aluminum with  $E_f/E_m \approx 0.556$ ), the error is 1.5% when  $r/a = 6$ ; (3) the observations made in (1) and (2) are true when circular markers are replaced by square markers of equivalent size; and (4) these results are valid both for uniaxial and biaxial loading cases shown in Figs. 5 and 6. However, in the case of fiber-reinforced composites, the results are valid for cases where the ratio of marker diameter to interfiber spacing is about 10%. For higher values of this ratio, say 50%, the local strain errors introduced by the markers are significantly higher because there is significant interaction between the fibers and markers' strain fields.

To illustrate the influence of moduli ratio on the local strain field, the error as a function of the modulus ratio is plotted in Fig. 11. In this figure, the error is normalized by the error that occurs for nickel markers placed five marker-diameters apart in an epoxy matrix. The error introduced by six markers, as shown in Fig. 12, was also studied. The results of these cases (Table 1) show that when the recommended spacing is maintained between two neighboring markers, their presence does not significantly influence the strain calculated using the markers as fiducial markers. In the actual sample, a marker typically has ten nearest neighbors as shown in Fig. 7. To compare the strain calculated using either marker A or B as a reference with the estimate given in Eq 11, we pair it with any three markers and use the standard strain gage rosette formula to calculate its in-plane strain components. The

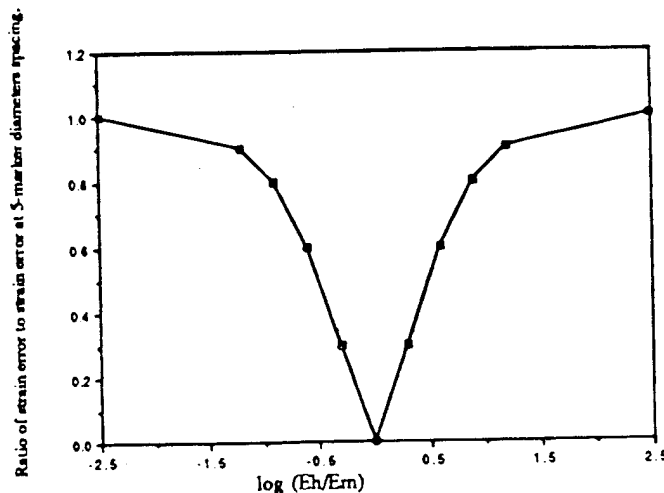


FIG. 11—Strain error ratio as a function of moduli ratio for a marker spacing of five marker diameters.

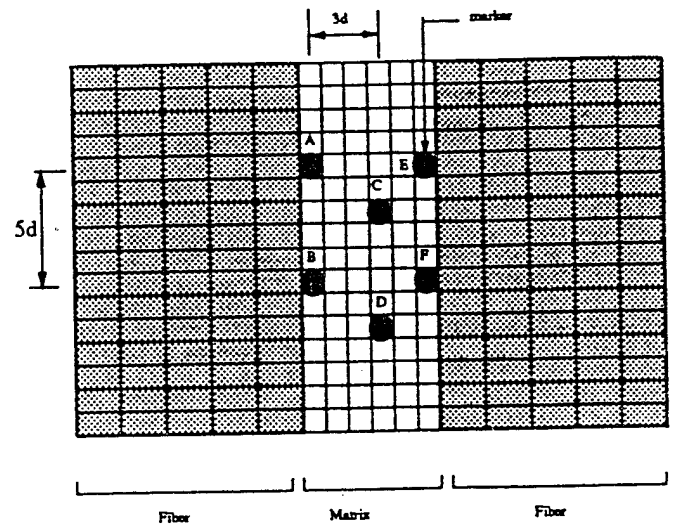


FIG. 12—Finite element model containing six markers.

results show that if the intermarker spacing is five marker diameters, the calculated strain values are within 2% and 0.5% of the applied strain for nickel-epoxy and gold-aluminum cases, respectively. Using Eq 11, the estimated errors are about 1.2% and 0.6%, respectively.

We also need to add that the principal stress concentration factor (SCF) for a rigid marker is 2 as also shown in Refs 13 and 14. The SCF calculated from FE is approximately 1.25 and 1.876 for gold-aluminum and nickel-epoxy material systems, respectively. These SCF factors are within 4% of the theoretical values. For relatively hard inclusions having a SCF of 2, one can infer that local yielding will occur if the host material is monotonically loaded to one half of its yield strength, while for moderate cyclic loading crack initiation may occur at the marker-host material interface. The cases studied here are better than those reported by Czarnek et al. [6] where the value of the SCF is 10.

In all the cases discussed thus far, the host material was only allowed to deform elastically. These do not represent all cases in practice, particularly because we can use the fiducial markers to measure strain fields in regions of high strain gradients, such as around holes, material interfaces, etc. For these cases, the host material could experience plastic deformations. In order to accommodate these cases, we also studied the strain error when the host material deforms plastically. The Ramberg-Osgood strain hardening law [17] was adopted for the plastic strain behavior of the host material. Our results show that in the plastic strain range, including cases with high (0.2) and low (0.02) strain hardening exponents, the strain error depends on the applied strain values. Specifically, for the aluminum sample containing two markers five marker diameters apart, the strain error is about 1.6% when the monotonically applied plastic strain is less than 50 times the initial yield strain. On exceeding this value, it is observed, as shown in Fig.

TABLE 1—Local influence of markers for host material containing six markers.

Marker Pair	Marker Spacing (marker diameters)	Average Strain Error, %
A-B	5	0.95
C-D	5	0.72
E-F	5	0.71

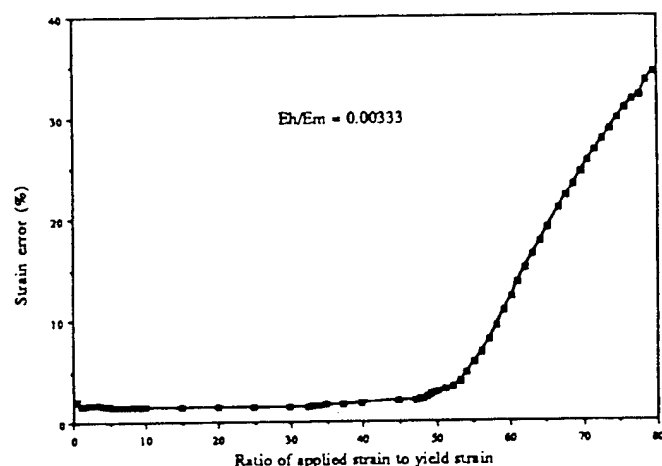


FIG. 13—Strain error in plastic strain region for aluminum host material containing two rigid markers.

13, that the strain error increases drastically and can be as high as 50%. The material was also observed to have strained considerably outside the region containing the markers which seemed reinforced by the relatively rigid markers. Also, in the plastic strain region, the value of strain concentration factor is about 1.4.

## Conclusions

The results of this study have shown that:

1. The global influence of the markers on the structural response of the host medium is negligible for marker-volume fractions less than 1%. Considering the fact that in the new experimental technique [4] the practical marker volume-fraction is approximately 0.11%, one can conclude that the global influence of the markers on the measured strain field is insignificant.
2. The local influence of the markers on the response of host medium is insignificant on the local average strain when the spacing between the markers is at least five marker diameters for very hard markers and three marker diameters for markers of moderate hardness. This is true when the material is deformed elastically as well as when it is deformed plastically provided that the applied plastic strain is less than 50 times the initial yield strain.
3. For elastic deformation, when the intermarker spacing is at least five marker diameters, one can use the solution of a medium containing two noninteracting markers (see Eq 10) to predict the behavior of the same medium containing two or more interacting markers.

4. The conclusions regarding the strain errors due to a pair of markers in a homogeneous or composite medium for markers that are five or more diameters apart also apply for multiple markers.

## References

- [1] Claus, R. O., Murphy, A., and Bennett, K. D., "Smart Skins and Structures," *Proceedings of the 1989 SEM Spring Conference on Experimental Mechanics*, SEM, Boston, 1989, pp. 528-533.
- [2] Valis, T., Hogg, D., and Measures, R. M., "Composite Material Embedded Fabry-Perot Optic Strain Rosette," *SPIE OE/Fibers 90-Conference: Fiber Optic Smart Structures and Skins III*, San Jose, CA, 16-21 September 1990.
- [3] Measures, R. M., "The Detection of Damage and the Measurement of Strain within Composite by Means of Embedded Optical Fiber Sensors," *Review in Progress of Quantitative Nondestructive Evaluation*, La Jolla, CA, 15-20 July 1990.
- [4] Jordan, E. H., Ochi, S. C. U., Pease, D., and Budnick, J. L., "Micro-Radiographic Strain Measurements Using Markers," *Experimental Mechanics*, June 1994, pp. 155-165.
- [5] Measures, R. M., Glossop, N. D. W., Lymer, L., et al., "Structurally Integrated Fiber Optic Damage Assessment System for Composite Materials," *Applied Optics*, Vol. 28, No. 13, July 1989, pp. 2626-2633.
- [6] Czarnek, R., Guo, Y. F., Bennett, K. D., and Claus, R. O., *Proceedings, SPIE O/E Fiber Laser*, Boston, MA, September 1988.
- [7] Haslach, H. W. Jr. and Whipple, K. G., "Mechanical Design of Embedded Optical Fiber Interferometric Sensors for Monitoring Simple Combined Loads," *Optical Engineering*, Vol. 32, No. 3, March 1993.
- [8] Christensen, R. M., *Mechanics of Composite Materials*, John Wiley and Sons, New York, 1979.
- [9] Hashin, Z. and Rosen, B. W., "The Elastic Moduli of Fiber-Reinforced Materials," *Journal of Applied Mechanics*, Vol. 31, No. 223, 1964.
- [10] Timoshenko, S. P. and Goodier, J. N., *Theory of Elasticity*, third ed., McGraw Hill, New York, 1970.
- [11] Goodier, J. N., "Concentration of Stress around Spheroidal, and Cylindrical Inclusions and Flaws," *ASME Transactions, Volume 55, Applied Mechanics*, 1933, pp. 39-44.
- [12] Chen, H. and Acrivos, A., "The Solution of the Equations of Linear Elasticity for an Infinite Region Containing Two Spherical Inclusions," *Journal of Solids and Structures*, Vol. 14, 1978, pp. 331-348.
- [13] Shelley, J. F. and Yu, Y. Y., "The Effects Two Rigid Spherical Inclusions on the Stresses in an Infinite Elastic Solid," *Journal of Applied Mechanics*, Vol. 33, 1966, pp. 68-74.
- [14] Tandon, G. P. and Weng, G. J., "Stress Distribution around Spheroidal Inclusions and Voids at Finite Concentration," *Journal of Applied Mechanics*, Vol. 53, 1986, pp. 511-518.
- [15] Savin, G. N., *Stress Concentration Around Holes*, Pergamon Press, New York, 1961.
- [16] Ochi, S. C. U., "Measurement of Internal Strains Using Synchrotron Radiation and Marker Particles," Ph.D. thesis, University of Connecticut, May 1992.
- [17] Meyers, M. A. and Chawla, K. K., *Mechanical Metallurgy: Principles and Applications*, Prentice-Hall, 1984.

## **Appendix II-Microradiographic Strain Measurement Using Markers-1st Generation Technique**

# Microradiographic Strain Measurement Using Markers

by E.H. Jordan, S.C.U. Ochi, D. Pease and J.I. Budnick

**ABSTRACT**—A method for measuring strain on interior planes of some real structural materials is presented. X-ray images are formed of small (10–40 micron) gold markers placed on selected interior planes of optically opaque X-ray transparent materials. The use of well collimated monochromatic synchrotron radiation makes possible high contrast images of the small markers. Images of the particles before and after straining are recorded photographically. Photographs are enlarged 33X and measured using a simple electro-optical setup. In calibration experiments using approximately a 300-micron gage length, the strain measured by this method agreed with extensometer measured strains to within 100 microstrain. Example applications in a graphite-epoxy composite are presented, including measurement of the strain drop off near the free edge, strain concentration around a hole, and the strain field on a particular plane near a hole after local delamination. The technique is currently limited to materials no less X-ray transparent than titanium.

## Introduction

The new technique<sup>\*</sup> presented here was specifically developed to study strain fields on interior planes of real structural materials that are optically opaque. The authors developed the technique out of an interest in measuring local strain fields in composites that can be calculated by various micromechanics methods. The two methods presently in use, which are most useful for measurement of strain on interior planes, are frozen-stress photoelasticity<sup>1</sup> and speckle holography.<sup>2</sup> Both of these techniques offer good strain and spatial resolution. However, they require that the sample be optically transparent. Many problems of interest involve opaque materials; it was for such materials that

this technique was developed. The new technique has a strain noise level that is at present inferior to the two optical techniques, and a comparable spatial resolution. Its importance is primarily in its ability to measure strain at interior locations in optically opaque materials.

Three other related techniques are worth mentioning before discussing the X-ray radiographic technique. X-ray diffraction methods are commonly used to measure surface residual stress by determining lattice constants through Bragg diffraction. The present technique uses entirely different physics from the diffraction-based methods and should not be confused with such methods. Second, neutron diffraction can be used to determine the average stress separately for the fiber and the matrix in a composite.<sup>3</sup> The present technique is capable of determining not only average stress values but also the distribution of strain with a spatial resolution of a few hundred microns. Third, the method used to extract strain from the radiographs is closely related to that employed by James *et al.*<sup>4</sup> to extract strain from surface photographs. The success of their technique influenced the choice of method for analyzing the radiographs.

In broad overview the new method works as follows. A sample is fabricated with small (5 to 50 micron) X-ray opaque (usually gold) markers on a plane upon which strain information is desired. Well collimated monochromatic intense X-rays from a synchrotron are used to form a radiographic picture of the location of the markers before and after a load has been applied. Relative displacement of the markers is determined using an electro-optical method. Strains are computed from the measured displacements. At present, gage lengths of about 300 microns are employed and the measured strain agrees with the strain determined by other methods to within roughly 100 microstrain. At present, the deviation of strain measured by the new method from that measured by established methods appears random and corresponds quite closely to the deviation expected from the observed fluctuation present in the electro-optical setup used to measure displacements.

*E.H. Jordan (SEM Member) is Professor, S.C.U. Ochi is Postdoctoral Research Assistant, D. Pease is Associate Professor, and J.I. Budnick is Professor, University of Connecticut, 191 Auditorium Road, U 139, Storrs, CT 06269-3139.*

*Paper was presented at the 1992 SEM Spring Conference on Experimental Mechanics held in Las Vegas, NV on June 8–11.*

*Original manuscript submitted: February 12, 1993. Final manuscript received: September 30, 1993.*

The procedure currently used to make these measurements is presented in detail. Because the technique is new, it is likely that it will be further refined. To facilitate that process and provide a rationale for particular procedures used, a discussion of the basic issues connected with X-ray image formation is also provided. An experimental study of different error sources is presented. Finally, example applications are shown involving polymer composite specimens.

## Description of the Technique

The technique consists of the following steps:

1. Fabrication of the sample with markers on the plane of interest.
2. Forming radiographic images of the marker positions before and after loading.
3. Measuring the relative displacement of the markers in the before and after images, and computing strain.

The specific techniques used for each of the above steps are presented below along with a general discussion of the problems associated with each step that lead to the specific method chosen.

## Specimen Fabrication

Radiographs will record the position of markers at all locations throughout the sample thickness. It is possible to put markers uniformly through the bulk of the sample and make measurements. However, such measurements would yield through-thickness averaged strain values that are generally not as interesting as strains on individual planes. Accordingly, all samples made to date have had markers on specific planes, which in most cases has been the midplane. Three methods have thus far been used to fabricate samples: (1) Surface markers have been attached by mixing marker particles with an epoxy and painting them on the surface. This method has been applied to aluminum and graphite epoxy samples. (2) Markers at interior locations have been installed in graphite epoxy composites by mixing the marker particles with a compatible epoxy and painting the markers on the surface of the prepregs. The composite sample with the marked prepregs is then heat consolidated in a hot press. (3) Aluminum boron composite samples have also been made by mixing markers with binder and painting foils with the marker loaded binder. In the hot pressing of metal matrix composites, it is important that the metal (gold) markers not go into solution during hot pressing. Gold markers of roughly 20 microns survived hot pressing of aluminum boron. The feasibility of making other hot-pressed composites will have to be demonstrated one system at a time.

All of the above methods involve making a mixture of marker particles in liquid where it is important that the mean spacing of the markers is about five particle diameters. Achieving such ideal mixtures is difficult and involves experimentation. In general, the liquid and markers are measured by weight and mixed in an electric laboratory mixer.

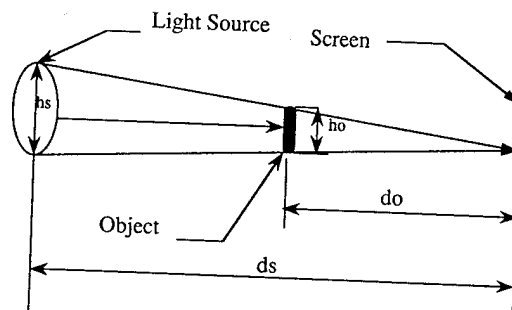
## Producing High-resolution Radiographs

It is desirable to produce high-resolution images of the smallest possible marker particles. Small particles will least disturb the strain field being studied and high spatial resolution is always desirable in strain measurement. It is also essential that any magnification or image distortion be the same in the before and after deformation radiographs. Any nonconstant distortion or magnification will be interpreted as strain and will be a source of error.

A serious consideration in strain measurement is the potential effect of markers on the strain field being measured. In the experiments done to date, the markers have much higher elastic moduli than the material into which they have been installed. Calculations were done<sup>5</sup> using both elasticity solutions and the finite-element method to see how close together the markers could be put before significant errors in strain measurement were produced. These studies yielded the result that as long as the markers were five diameter apart the measured strain would be less than one percent in error due to the influence of the markers on the strain field.

Because of the requirement of five diameters separation, shorter gage lengths require the use of smaller particles. The ultimate resolution possible in radiography is quite impressive. Images of objects less than 0.0050 microns<sup>6</sup> have been successfully recorded. Such high-resolution radiographs involved small objects sitting directly on the surface of the film, and soft X-rays were used. In the current application, two problems arise that prevent the achievement of such high spatial resolution. The first problem is that markers embedded in a sample must be a finite distance from the film. With imperfect collimation of radiation, the shadow will fill in as in Fig. 1. The second and more limiting problem is that, for the present, radiation must be sufficiently energetic to penetrate the sample thickness. Thus, markers that are thinner than some minimum thickness are too transparent to form an observable image.

The 'shadow fill-in' problem is minimized by using a well collimated radiation source. The best such source



From Similar triangles  $h_o = h_s \times (d_o/d_s) = \text{minimum object size}$

Fig. 1—Imaging with uncollimated light source

is synchrotron radiation. Synchrotron radiation may be thought of as a finite source on the order of 1 mm in size.<sup>7</sup> Typically the apparatus is 12 m from the source. Geometric consideration for such a setup shows that shadow fill-in occurs when a 1-micron marker is 12 mm from the film. In experiments done to date, the film-to-marker distance has usually been only a few millimeters. As will be seen in the next paragraph, this problem is not the limiting one.

The contrast problem can best be explored using the Beer-Lambert law of absorption given below.

$$\frac{I_t}{I_0} = \exp(-\mu x) \quad (1)$$

If the ratio of intensity of the radiation that passed through the marker,  $I_t$ , to the incident radiation  $I_0$ , is too close to one, there will be insufficient contrast to see the marker on the film. In eq (1), it is obvious that the best marker is the one with the highest absorption coefficient  $\mu$  at the wavelength of radiation being used. Because of the interaction of photon energies and electron band gap energies, absorption coefficients have peaks at certain energies for different elements. Experiments are run using radiation at the absorption peak of the chosen target material. The combination of availability of powders, toxicity, cost and X-ray absorption behavior found in Ref. 8 led the authors to choose gold as a favorable marker material. The gold powder used is from a commercial source and consists of irregularly shaped gold particles that must pass through a 10-micron mesh. Such particles may have a major axis length of as much as 30 microns. In principle, it is possible to estimate the required thickness for the markers using eq (1). However attempts to do this were never consistent with experiments. We suspect that eq (1) does not allow quantitative predictions because small unknown amounts of higher energy and highly penetrating X-rays (harmonics) are always present in beams coming from single crystal monochrometers. Minimum marker thicknesses were determined experimentally.

In addition to having sufficient contrast in forming the image of markers, it is also necessary that enough radiation passes through the sample to allow photographs to be taken in a reasonable time. Generally, materials become more absorbing as atomic number increases while X-rays become more penetrating as the photon energies increase. Equation (1) and the data in Ref. 8 can be used to estimate acceptable thickness for various materials. Recognizing the inexact nature of such calculation due to the influence of harmonics, these calculations are of qualitative use. For example at the 14.14-KeV absorption edge of gold the allowable thicknesses are estimated to be 2.7 mm and 25.6 mm for aluminum and carbon respectively. This calculation is based on needing  $1.2 \times 10^9$  photons/cm<sup>2</sup> on the film, 30-seconds exposure and a typical synchrotron source brightness of  $2.5 \times 10^9$  photons/s-cm<sup>2</sup>.

The ideal film for this application must have high spatial resolution. It is desirable for it to have high

contrast and a high film speed to minimize exposure time. The film selected, Industrex-R, is an industrial radiographic film, which according to the manufacturer, is capable of recording between 2000 and 6000 line pairs/mm.

The setup used to make radiographs is shown in Fig. 2. In order to take before and after loading radiographs, a small portable hydraulic load frame was designed and built specifically to fit into the safety enclosure at the synchrotron.

### Displacement Measurement from Radiographs

In order to determine strain from the before and after radiographs, it is necessary to measure quite accurately the change in spacing of the markers. The current strain resolution of 100 microstrain requires measurement position to 1 part in 10,000. A substantial number of possible methods for this step in the technique were considered including the use of Young's fringes,<sup>9</sup> digital image correlation,<sup>10</sup> several variations of interferometric methods related to Sharpe's method,<sup>11</sup> and finally, a direct method using position-sensitive photodiodes which is related to the method of James *et al.*<sup>4</sup> The method which uses position-sensitive photodiodes was chosen. Such a method uses individual pairs of markers, which yield the shortest gage length possible; and it appeared to be the easiest method to implement successfully.

The first step in making marker-position measurements is to make a 33X enlarged positive slide picture of the radiograph. This slide is made using a photo-optical microscope. It is important that the enlarged image be a positive one in order to end up with white dots on a dark background. Figure 3 shows typical marker images at 100X magnification. In making the enlargements, it is essential that the corresponding markers in the before and after images be recorded in the same part of the field of view of the microscope. The magnification of the microscope used is only specified to be uniform to 1 part in 100. Failure to carefully locate markers in the same portion of the field of view could potentially result in the recording of a fictitious noise strain of up to 10,000 microstrain. In making the enlargements, it is critical to have the before and after image located identically with respect to the microscope field of view. In most cases a double-exposure technique was used in which the before and after image were recorded on a single piece of film. A single-exposure method was also sometimes used with equally good results.

The second step in the measurement process used the setup shown in Fig. 4. The enlargements were mounted on a high-resolution manual x-z stage. A 10 mW He-Ne laser beam 0.68 mm in diameter was passed through the slide. An image of the back side of the illuminated slide was formed on a position-sensitive lateral effect photodiode using a camera lens with added macro lenses. The photodiode yields a null reading whenever the centroid of a dot of light is centered on it. An optical filter is placed over the photo detector which blocks all light except at the wave-

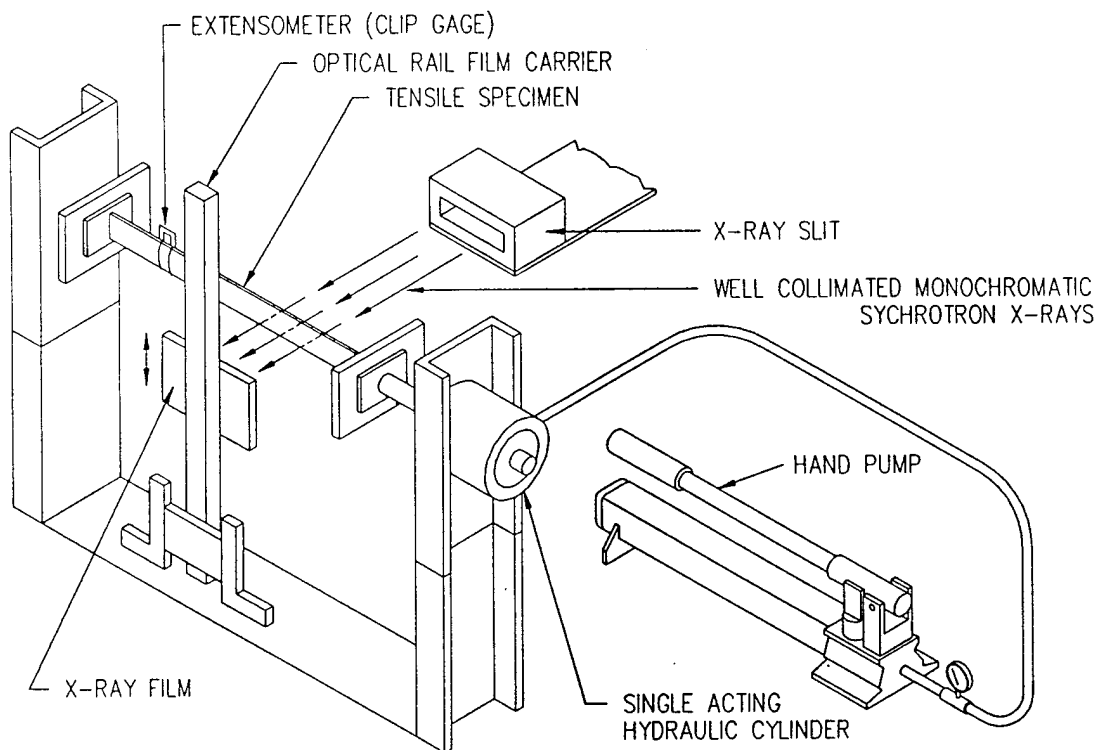


Fig. 2—Schematic of experimental tensile testing equipment

length of the laser. This filter reduces the disturbances from ambient light fluctuations.

The x-z position of each dot from the x-z micrometers after each dot is centered in front of the lateral-effect photodiode. The micrometers read to 1.0 micron. The lateral-effect photodiode has specified sensitivity of 1 micron. In this setup, there is instability second to second of about 1 micron. This instability appears to limit our measurement accuracy and repeatability. Note that 1-micron position uncertainty on a 33X enlargement corresponds to a 0.03-micron uncertainty on the original radiograph. With a 300-micron gage length in the original radiograph, the strain uncertainty is 100 microstrain which is approximately the uncertainty in the calibration experiments reported later in this paper.

### Calculation of Strain

The method chosen for the calculation of strain is the simplest possible method. Normal strains were calculated from the change in separation of individual marker pairs. A single dot was paired with three others to form a rosette. Standard rosette formulas were used to calculate the in-plane strains. The relatively sparse data collected in these initial experiments did not warrant the use of more sophisticated methods<sup>11</sup> of calculating strain from displacement data.

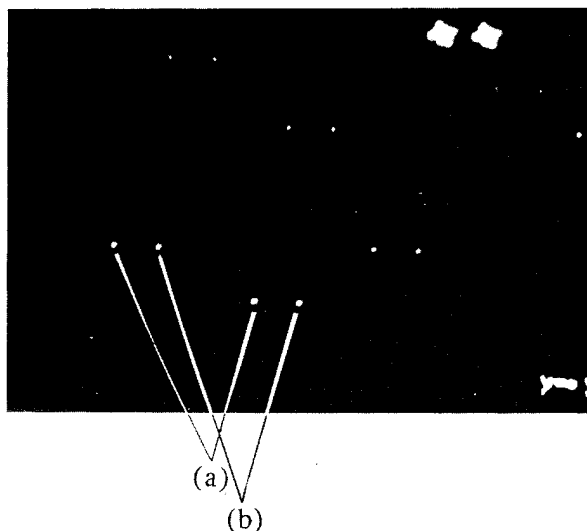


Fig. 3—100 X photo of positions of gold markers as seen through 1.25 mm of aluminum (6061-T: Markers images (a) before deformation and (b) after 0.00220 strain deformation)

### Quantifying and Controlling Sources of Error

In the present method, strain is determined from accurate position measurements using photographic

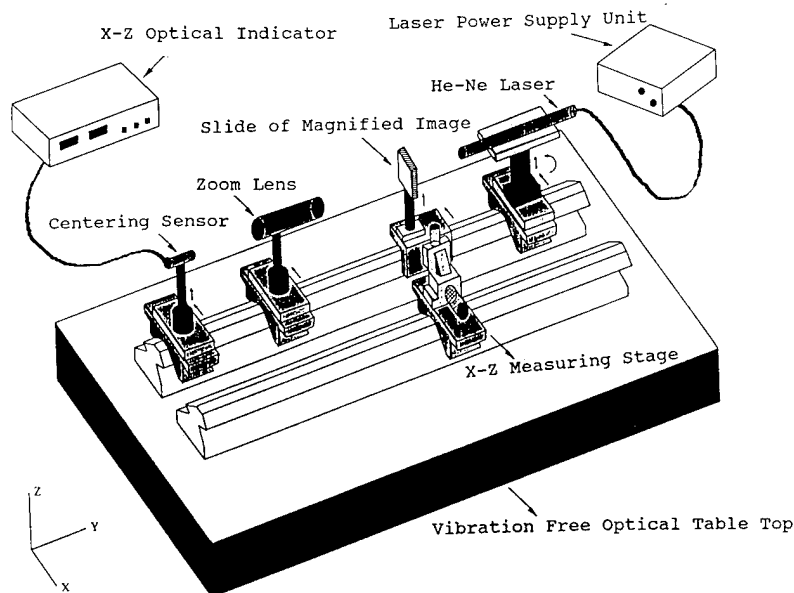


Fig. 4—Electro-optical system for measurement of inter-marker spacings

images taken before and after deformation. Any difference in magnification or in image distortion between the before and after deformation images will appear as a fictitious strain. The error due to image distortion is potentially large and was studied experimentally. As mentioned earlier, the electro-optical method used to extract position information yields a strain error of about 100 microstrain when a 300-micron gage length is used. Since the electro-optical setup is used in the experimental investigation of error, any errors much smaller than 100 microstrain could not be studied. The distortion introduced when making the X-ray photos was too small to study because of this limitation. Two steps were taken to minimize any error when recording the X-ray images: first, the X-ray film was held flat in a film holder when making the radiographs, and second, the before and after images were taken near each other on the same piece of film to minimize differential film shrinkage. Originally, glass X-ray plates were used to minimize distortion in the X-ray images; however, the X-ray plates were expensive, required longer exposures, and most importantly, the image faded from the plates in less than a month.

Measurement of strain noise sources other than those from the recording of radiographs was undertaken. To do this, a single radiograph taken before deformation was used. This radiograph was used as both the before and after deformation image. Since no deformation actually occurred, all nonzero strains were false strains. The markers on the original radiograph were typically 250 microns apart. Except where noted, all distances are given for the original radiograph and not the 33X enlargement.

### Focussing Errors

It was found that satisfactory results required holding the radiograph flat when making enlargements. This was accomplished by gluing the radiographs between two glass slides. In making the before and after enlargements, two procedures were possible. The focus could be locked and both images recorded at a fixed focus, or the focussing could be redone for each image. An experiment was conducted in which the same region of a radiograph was enlarged four different times, refocussing after each enlargement. The false strain caused by refocussing was more than double that found using a locked focus and consequently, locked focussing was always used.

### Nonuniform Magnification Error

Based on microscope specifications, nonuniform magnification can produce errors of up to 10 000 microstrain. To explore this error, the false strain caused by moving the radiograph one-half of a field of view between the before and after enlargements was found. The results of three repetitions of this procedure are shown in Table 1.

To remove this error a microscope eyepiece with a movable crosshair was used to get images accurately located in the same part of the field of view when making enlargements.

### Overall False Strain Using the Current Technique

From the above, it is clear that locked focus should be used along with careful positioning of the radio-

TABLE 1—FALSE STRAIN FROM NONUNIFORM MAGNIFICATION UNDER ONE-HALF FIELD OF VIEW OFFSET

Average false strain in three trials = 236 microstrain  
Maximum false strain in three trials = 622 microstrain

TABLE 2—STRAIN ERROR IN SINGLE- AND DOUBLE-EXPOSURE ENLARGEMENT TECHNIQUE

	Single Exposure	Double Exposure
Average false strain	38 microstrain	37 microstrain
Maximum false strain	77 microstrain	63 microstrain

graphs in the microscope field of view. To compare the double-exposure and single-exposure method, and to show the false strain present when the technique is used in its current form, experiments were run involving four measurements of false strain for the single-exposure method and ten measurements using the double-exposure method. The results are given in Table 2.

The above results show that the error using locked focus and careful alignment of the corresponding regions in before and after photos yields a maximum error of around 70 micro strain.

#### Direct Comparison with Extensometer Strains

It is important to obtain strain values that are verified by another technique. Here we choose to com-

pare our results with results obtained using a commercial 12.7-mm gage-length strain-gage extensometer (ASTM-8). The calibration specimen was a 1.25-mm thick pure aluminum tensile sample which had a dog-bone shape and a uniform section 130-mm long. Gold markers 10 to 30 microns in size were applied to the surface using epoxy. The mean particle spacing was about 300 microns. The mean particle spacing is at least 10 particle diameters, which is more than sufficient spacing to make the influence of the particle on the measured strain less than one percent. Note that the X-rays pass through the full sample thickness as they would in internal strain measurement. The sample was tested, using the setup described in Fig. 2, and the radiographs were analyzed using the double-exposure method with locked focusing as discussed in the previous section. A plot of the strain measured by the present X-ray method versus the extensometer strain is shown in Fig. 5. In Fig. 5 it can be seen that the variation in strain between maximum and minimum seems to be roughly independent of strain value as would occur with the observed position noise in the electro-optical setup. The maximum strain is approximately 4300 microstrain. A summary of the errors is presented in Table 3.

TABLE 3—DIFFERENCE BETWEEN X-RAY DETERMINED STRAIN AND THE EXTENSOMETER STRAIN

Maximum strain difference = 400 microstrain  
Average strain difference = 65 microstrain

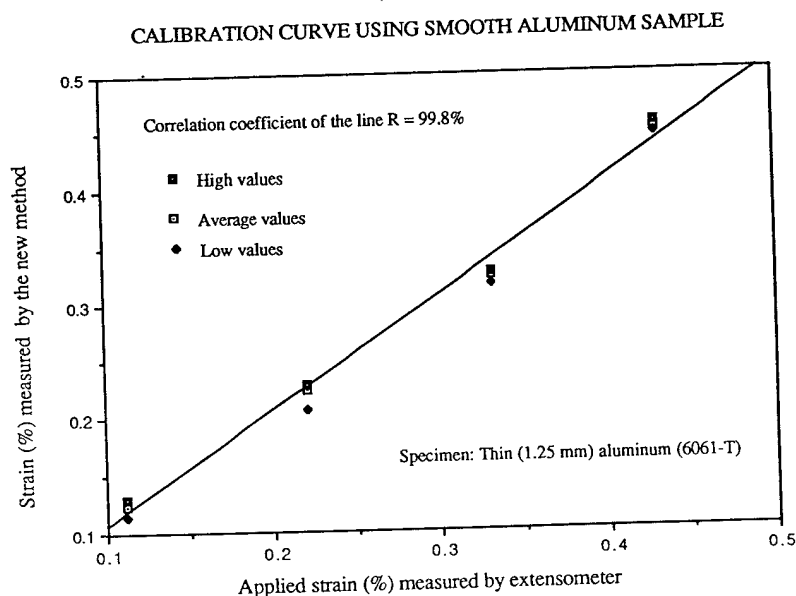


Fig. 5—Comparison of aluminum sample's strain measured by radiography with that by extensometer

Finally, it was also possible to determine an average Poisson's ratio which turned out to be 0.27. This is close to the handbook value of 0.3.

The radiographs of this sample showed that it had porosity which may have effected some of the specific readings, possibly exaggerating the maximum error.

### Application Experiments

Using the new method, two application experiments were conducted using graphite-epoxy composites, namely: (1) measurement of in-plane interlaminar strains in smooth samples, and (2) measurement of in-plane interlaminar strain concentrations near a hole.

The measurement equipment which was used for the calibration experiment was also used for these application experiments. Here, the specimens consisted of rectangular 6 mm  $\times$  1.25 mm strips which were cut from  $[+45/-45/-45/+45]_s$  graphite-epoxy laminate. Randomly distributed gold markers were glued onto the prepreg lamina prior to consolidation bonding. The prepreg containing the markers was placed in the middle of the stack during the lamination. The markers were therefore located in the mid-plane of the laminate. Two sample types were prepared: one without a hole, and other with a central-through hole of

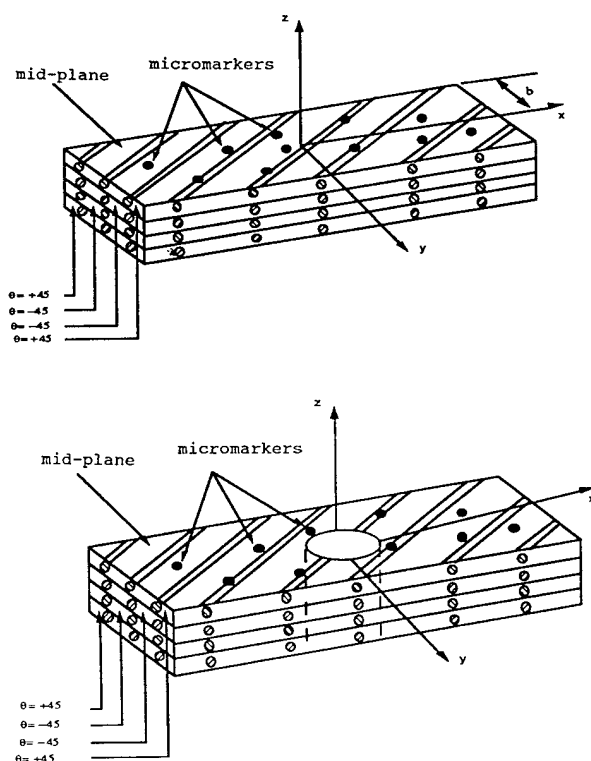


Fig. 6—Schematics of bottom-half geometry of composite sample (a) without hole and (b) with hole, showing micromarkers on the midplane of the samples

6.35-mm diameter. Schematics of the test-specimens are shown in Fig. 6.

In the applications, radiographs of the markers at various locations in the two specimens were recorded before and after deformation using synchrotron X-rays. A typical magnified double-exposure (100X) picture of the markers as seen inside the laminate is shown in Fig. 7.

The differential displacement information was extracted using exactly the same procedure as described in the calibration experiment. Like the calibration experiment, the nominal strain was measured by a 12.7-mm gage-length extensometer mounted on one side of the center of the specimen.

For the smooth samples, the in-plane strains in the midplane as well as those located near the free edge were determined using the new technique and compared to theoretical calculated strains deduced from theoretical stresses given in Refs. 12–14. The results are discussed in the following section. Similarly, for samples with hole, measured near-hole strain concentrations were compared with theoretical results as given in Refs. 15–16. They are discussed in 'Results and Discussions of Composite Samples with Hole' below.

### Results and Discussions of Smooth Composite Samples

A plot of the internal strain measured at the center line of smooth composite sample versus the extensometer strain is shown in Fig. 8. From the figure it can be seen that the average difference is 55 microstrain and the maximum difference is 100 microstrain which is better than the calibration experiment in 'Direct Comparison with Extensometer Strains' above

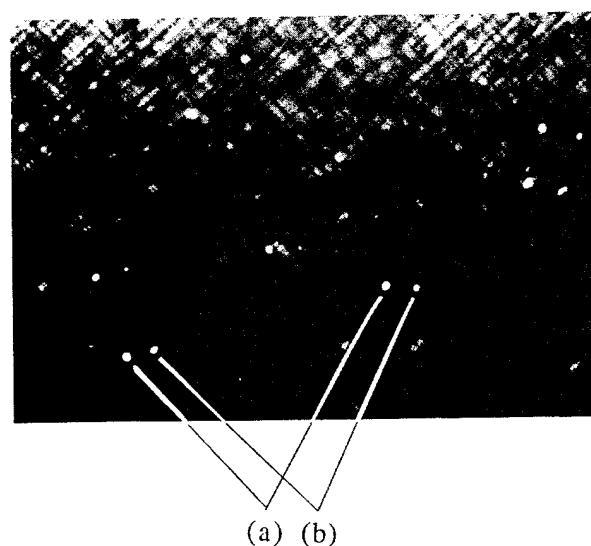


Fig. 7—100 X photo of positions of gold markers as seen on the midplane of 1.25 mm of graphite-epoxy composite: Markers images (a) before deformation and (b) after 0.00350 strain deformation

# CALIBRATION CURVE USING GRAHITE-EPOXY COMPOSITE

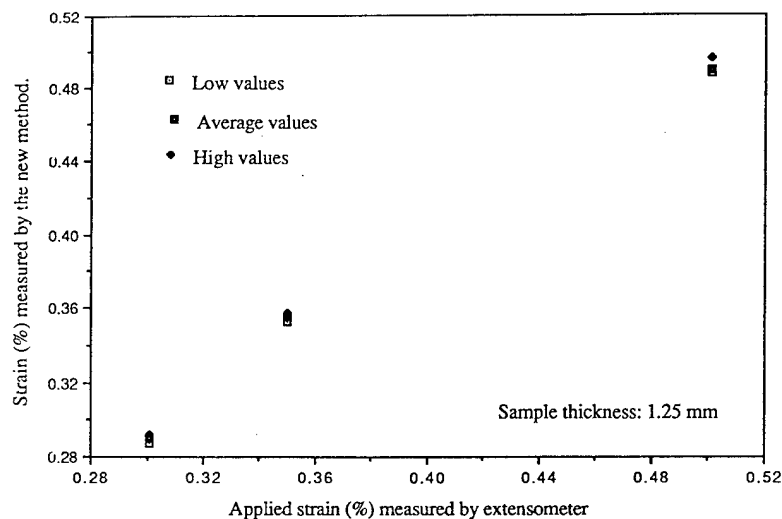


Fig. 8—Comparison of composites' internal strain measured by radiography with that by extensometer

lending credence to the possible adverse influence of the observed porosity in the calibration experiment.

To generate additional discussion of the results, the measured strains are compared to the strains deduced from the theoretical works of Pipes and Pagano;<sup>12</sup> Kassapoglou and Page;<sup>13</sup> and Wang and Crossman.<sup>14</sup> These authors worked on similar laminated  $[-45/+45]_s$  graphite-epoxy composites. These strains were calculated from the theoretical stress results using nominal values of the mechanical properties ( $E_{11} = 138$  GPa,  $E_{22} = 14.4$  GPa,  $G_{12} = 5.9$  GPa, and  $\mu_{12} = 0.21$ ) of the composite. The same mechanical properties were assumed for the test samples.

The strains measured by the new method and the strains calculated from Refs. 12–14 are shown in Table 4, where it can be observed that the measured axial strains are within  $\pm 2$  percent of the extensometer strains. Also, the shear strain components are negligible in both the experimental and theoretical results. Furthermore, the Poisson's ratio  $\mu_{xy}$  is  $-0.75$  for theoretical results, while its average value is  $-0.392 \pm 0.0146$  for the experiment results.

In understanding the results, it is important to keep in mind the idealization used in the theoretical analysis and how it differs from the actual experiment. In each theoretical analysis, the composite is assumed to consist of a stack of perfectly bonded orthotropic lamina with the elastic properties obtained from an averaging process. In the theory, there is no location having the pure matrix properties or the pure fiber properties. In the experiment, because of the fabrication technique, the markers are in a thin, pure matrix layer. One can therefore speculate that the large difference between the predicted and measured Poisson's strains is due to this difference between the idealized model and the real specimen.

Strains were also examined near the free edge where theoretical solutions<sup>12–14</sup> predict a drop in strain from that found on the center line. The theoretical solutions reported in Refs. 12–14 are for four-layer symmetric  $\pm 45$  lay-up while our experimental results are for the same lay-up with eight layers. Only qualitative comparison is possible. Table 5 and Fig. 9 show the comparison between theory and experiment. The experi-

TABLE 4—INTERNAL IN-PLANE STRAINS MEASURED AT THE CENTER LINE OF GRAPHITE-EPOXY COMPOSITE

Applied Strain	Average Measured Strains Normalized w.r.t. Applied Strain			
	Axial	Transverse	Shear	Poisson's Ratio
0.00301	0.9767	-0.338	-0.0282	$-0.346 \pm 0.015$
0.00350	1.0145	-0.428	-0.0240	$-0.422 \pm 0.017$
0.00501	0.9780	-0.401	-0.0339	$-0.410 \pm 0.012$
Theoretically Deduced Strains from Refs. 12–14 Normalized w.r.t. Applied Strain	0.994	-0.747	-0.0014	-0.75

TABLE 5—INTERNAL IN-PLANE STRAINS MEASURED AT NEAR EDGE (AT  $y/b = 0.90$ ) OF GRAPHITE-EPOXY COMPOSITE

Applied Strain	Average Measured Strains Normalized w.r.t. Applied Strain			Ref.
	Axial	Transverse	Shear	
0.00158	0.900	-0.318	-0.0092	
0.00506	0.962	-0.308	-0.0227	
0.00523	0.961	-0.398	-0.0256	
Theoretically Deduced Strains Normalized w.r.t. Applied Strain				
	0.923	-0.663	-0.0118	12
	0.835	-0.618	-0.0360	13
	1.240	-0.906	-0.0380	14

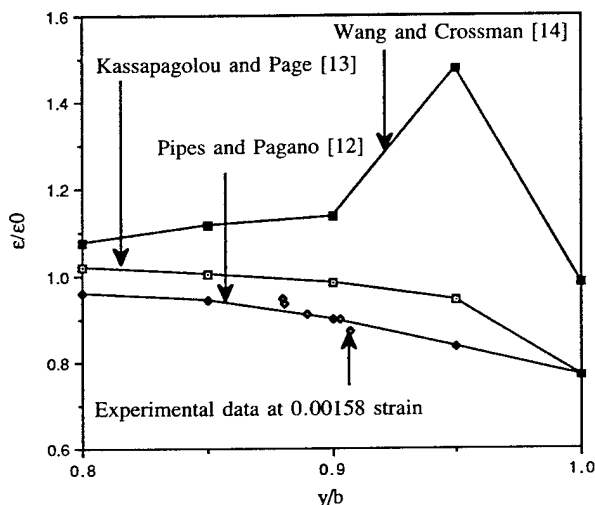


Fig. 9—Strain distribution near the edge in a smooth specimen

mental results in Table 5 and Fig. 9 support the presence of lower strains near the free edge. There is no indication of the local increase predicted by Wang and Crossman.<sup>14</sup>

### Results and Discussions of Composite Samples with Hole

The strain-concentration distribution near the hole was determined experimentally for two levels of nominal strain, an elastic strain of 3000 microstrain and a near-delamination strain of 7900 microstrain. A plot of the measured strain concentrations at regions A and B is shown for elastic loading in Fig. 10 together with plots of equivalent theoretical results from exact orthotropic solutions by Lekhnitskii<sup>15</sup> and extended orthotropic approximate solution by Konish and Whit-

ney.<sup>16</sup> The theoretical results are also for  $[\pm 45]$ , graphite-epoxy composite. From Fig. 10, one can observe that the experimental results are consistently closer to the results given in Ref. 16, while slightly deviating from those given in Ref. 15. Note that the highest strain concentration for these elastic strains' cases is approximately 2.2.

It is worth noting that in the experiment, the variation of the strain was obtained within 162 microns of the edge of the hole for region A and within 362 microns of the hole's edge for region B. These results illustrate the use of the good spatial resolution of the technique in a case involving a steep strain gradient.

The results of second case showing the measured strain concentration for the near-delamination strain are plotted in Fig. 11. From the results in Fig. 11, one can observe the following: strain concentration is 7.62 at about 137 microns from the hole; it rises to 10.72 at about 500 microns from the hole; and drops to about 8.66 at about 908 microns from the hole. The sudden change in strain concentration to such large values must be due to local damage. Specifically, the strain concentration is lowest very close to the hole where the material is likely to experience the most damage, and it rises to higher values slightly away from the hole where the material is less damaged. This indicates that there is a load transfer from the weaker zone of the material to stronger zone. Note that the highest strain concentration is about five times that of the elastic strain case.

The strains near the free edge in the plane of the hole were also determined using the new technique and the strain concentration at this location ranged from 0.88 to 0.99 which is consistent with theoretical predictions for undamaged specimen with a hole.

The strain measurements revealed material damage that was not detected visually. More important, the nature of strain disturbance measured would be difficult to compute even in the unlikely event that the geometry of debonding and cracking could be determined. The new technique is a good way to examine strain fields in the interior of locally damaged samples which cannot be computed or easily be determined by other techniques.

### Conclusions

A novel method of measuring strains in the interior of real structural materials has been developed. The method involves the use of a synchrotron X-ray source to record images of micromarkers (10–30 microns) embedded in real structural materials. Measurement of the change in the relative position of the markers in the undeformed and deformed state allowed strain to be calculated. These position measurements were made, using an electro-optical setup.

Best results from the technique require careful consideration of focusing errors and errors caused by the nonuniform magnification of the microscope. Verification experiments show that the technique which currently uses gage lengths of approximately 300 microns has a strain error of  $\pm 100 \mu\epsilon$ . The technique

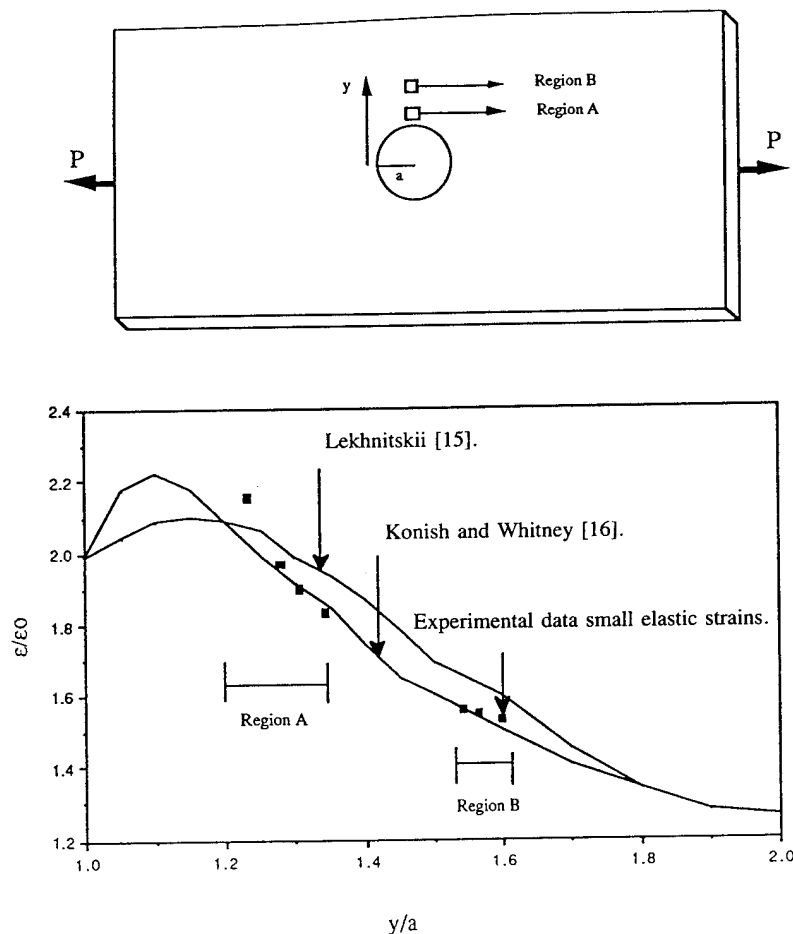


Fig. 10—Elastic strain concentration near the hole in regions A and B

has been used to measure strains in the interior of polymer composites and surface strains in aluminum. In preliminary experiments gold markers have been successfully installed during the hot-press fabrication of aluminum-boron composites. Markers have also been successfully imaged through 1.25-mm Ti-SiC composites. The technique is new and further improvements in performance are to be expected, especially with respect to gage-length reduction.

In the first example application presented, strains inside a polymer composite are measured, and the predicted drop in strains near the free edge compared to the center line is confirmed. In the second example application, near-hole strain concentrations inside the composite are measured for both an elastic loading and a near-delamination loading. Strain concentrations measured when elastic strains were applied agree well with predictions, while strain concentrations measured when near-delamination strains were applied show the method's ability to reveal strain fields associated with local damage that are difficult to compute.

#### Acknowledgments

We are very grateful to the following people: Dr. Gerry Lamble, Mr. Dale Brew, and Dr. Tan Zhou for their help with the synchrotron beam lines at Brookhaven National Laboratory (BNL); Mr. Tom Marcelino and his team at the mechanical workshop at UCONN for fabricating the rigs for the project; Mr. Craig Musson and C.G. Phippen of Pratt and Whitney for fabricating the composite samples, and for the extended loan of the optical indicator; and Dr. Robert Best for his help with the darkroom facilities at BNL. We further acknowledge the vital importance of access to the Cornell High Energy Synchrotron Source (CHESS) and the invaluable assistance of the CHESS operators.

This work was supported in part by DOE, contract Nos. DE-AS05-80ER10742 and DE-F602-90ER45424, and funded by the UCONN School of Engineering and the UCONN Research Foundation grant No. 35-283. Further development of this work is currently being funded by Air Force Office of Scientific Research (AFOSR) through grant No. F49620-92-J-0204.

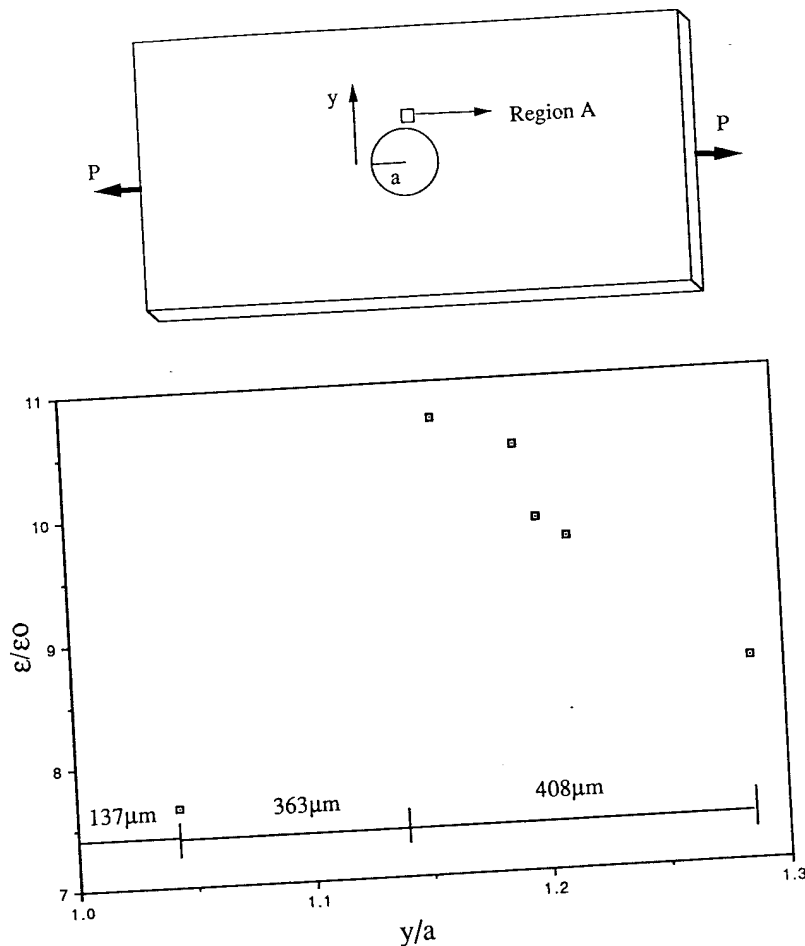


Fig. 11—Near-delamination strain concentration near the hole in region A

### References

1. Burger, C.P., "Photoelasticity," *Experimental Mechanics*, ed. by A.S. Kobayashi, Prentice-Hall, Englewood Cliffs, NJ (1987).
2. Chiang, F.P. and Kheaton, R.P., "Strain Analysis by One-Beam Laser Speckle Interferometry 2: Multiaperture Method," *Appl. Opt.* **18** (13), 2175–2186 (1979).
3. Kupperman, D.S., Majumday, S. and Singh, J.P., "Neutron Diffraction NDE for Advanced Composites," *Trans. of ASME, J. Eng. Mat. and Tech.*, **112**, 188–201 (1990).
4. James, M.R., Morris, W.L. and Cox, B.N., "A High Accuracy Automated Strain Field Mapper," *EXPERIMENTAL MECHANICS*, **20** (1), 60–67 (March 1990).
5. Ochi, S.C.U., "Measurements of Internal Strains Using Synchrotron Radiation and Marker Particles," PhD Thesis, Univ. of Connecticut (May 1992).
6. Feder, R., "High Resolution Soft X-Ray Microscopy," *Science*, **197** (1977).
7. Finkelstein, private communication (Dec. 1992).
8. McMaster, W.H., Kerr Dell Grande, N. and Mallet, J.H., "Compilation of X-Ray Cross Sections," Lawrence Radiation Lab. Rep. No. UCRL-50174 (1969).
8. Chiang, F.P., Adachi, J., Anastasi, R. and Beatty, J., "Objective Laser Speckle Method and its Application to Solid Mechanics," *Opt. Eng.*, **21** (5), 379–390 (1982).
9. Peters, W.H. and Ranson, W.F., "Digital Imaging Techniques in Experimental Stress Analysis," *Opt. Eng.*, **21** (3), 427–431 (1982).
10. Sharpe, W.N., Payne, T.S. and Smith, M.K., "Biaxial Laser-Based Displacement Transducer," *Rev. of Sci. Instr.*, **46** (6), 741–745 (1978).
11. Rowlands, R.E., Liber, T., Daniel, I.M. and Rose, P.G., "Higher-order Numerical Differentiation of Experimental Information," *EXPERIMENTAL MECHANICS*, **13** (3), 105–113 (1973).
12. Pipes, B. and Pagano, N.J., "Interlaminar Stresses in Composite Laminates Under Uniform Axial Extension," *J. Comp. Mat.*, **4**, 538–548 (1970).
13. Kassapoglou, C. and Page, P.A., "Closed Form Solutions for the Interlaminar Stress Field in Angle-Ply and Cross-Ply Laminates," *J. Comp. Mat.*, **21**, 292–308 (1987).
14. Wang, A.S.D. and Crossman, F.W., "Some New Results on Edge in Symmetric Composite Laminate," *J. Comp. Mat.*, **11**, 92–106 (1977).
15. Lekhnitskii, S.G., *Theory of Elasticity of Anisotropic Body*, Holden-Day, San Francisco (1963).
16. Konish, H.J. and Whitney, J.M., "Approximate Stresses on Orthotropic Plate Containing a Circular Hole," *J. Comp. Mat.*, **9**, 157–166 (1975).